Copy
RM L50I09

NACA RM L50I09

NACA

RESEARCH MEMORANDUM

A TRANSONIC WING INVESTIGATION IN THE LANGLEY 8-FOOT HIGH-SPEED TUNNEL AT HIGH SUBSONIC MACH NUMBERS AND AT A MACH NUMBER OF 1.2

WING-FUSELAGE CONFIGURATION HAVING A WING OF 35° SWEEPBACK, ASPECT RATIO 4, TAPER RATIO 0.6, AND NACA 65A006 AIRFOIL SECTION

By Beverly Z. Henry, Jr.

Langley Aeronautical Laboratory
Langley Air Force Base, Va.

CLASSIFIED DOCUMENT

NATIONAL ADVISORY COMMITTEE
FOR AERONAUTICS

WASHINGTON

November 15, 1950

NACA RM L50J09

NATIONAL ADVISORY COMMITTEE FOR AERONAUTICS

RESEARCH MEMORANDUM

A TRANSONIC WING INVESTIGATION IN THE LANGLEY 8-FOOT HIGH-SPEED TUNNEL AT HIGH SUBSONIC MACH NUMBERS AND AT A MACH NUMBER OF 1.2

WING-FUSELAGE CONFIGURATION HAVING A WING OF 35° SWEEPBACK, ASPECT RATIO 4, TAPER RATIO 0.6, AND NACA 65A006 AIRFOIL SECTION

By Beverly Z. Henry, Jr.

SUMMARY

As a part of a National Advisory Committee for Aeronautics research program, this paper presents the results of an investigation to determine the aerodynamic characteristics of a wing-fuselage configuration employing a wing with quarter-chord line swept back 35°, an aspect ratio of 4, a taper ratio of 0.6, and an NACA 65A006 airfoil section. Lift, drag, and pitching-moment characteristics, downwash angles, and wake characteristics for various angles of attack at high subsonic Mach numbers and at a Mach number of 1.2 are presented. These characteristics are presented for the wing-fuselage configuration and the wing and wing-fuselage interference.

Results at low lift coefficients indicated a decrease in lift-curve slope above a Mach number of 0.93, and an increase in drag coefficient above a Mach number of 0.90. Above a Mach number of 0.85 at low lift coefficients, the configuration experienced an increase in static longitudinal stability. At high angles of attack, abrupt unstable movements of the aerodynamic center were noted. Changes in trim at moderately low angles of attack near zero lift between Mach numbers of 0.96 and 1.2 can be expected as a result of corresponding variations in downwash.

Wake characteristics indicated that a horizontal tail located at the rear of the configuration should not be placed between 0.125 and 0.250 semispan above the wing-chord plane.

INTRODUCTION

As a part of an NACA research program, a series of wing-fuselage configurations is being investigated in the Langley 8-foot high-speed tunnel to study the effects of wing geometry on the aerodynamic characteristics at transonic speeds. The first phase of this program is a general investigation of the effects of sweep angle. The initial investigation of the sweep series was of a wing with quarter-chord line swept back 45° and is reported in reference 1. A comparison of results obtained in this series of tests with results for similar configurations obtained by various techniques in the Langley high-speed 7- by 10-foot tunnel is presented in reference 2.

This paper is the second in the sweep series and presents the results of an investigation of a wing-fuselage configuration employing a wing with 35° of sweepback referred to the quarter-chord line, an aspect ratio of 4, a taper ratio of 0.6, and an NACA 65A006 airfoil section measured parallel to the plane of symmetry.

For this investigation, lift, drag, and pitching-moment characteristics were determined for various angles of attack through a Mach number range from 0.6 to 0.96 and at a Mach number of 1.2. Wake characteristics and downwash angles were obtained at the rear of the configuration for two spanwise locations at various distances above the wing-chord plane.

SYMBOLS

C_D	drag coefficient $\left(\frac{D}{qS}\right)$
C_L	lift coefficient $\left(\frac{L}{qS}\right)$
C_m	pitching-moment coefficient $\left(\frac{M_{\bar{c}/4}}{qS\bar{c}}\right)$
$\bar{c}$	wing mean aerodynamic chord
D	drag
ΔH	total pressure loss in wake
L	lift
l	fuselage basic body length

[redacted]

M	Mach number
$M_{\bar{c}/4}$	pitching moment
P_b	base-pressure coefficient $\left(\frac{p_b - p_o}{q}\right)$
p_b	static pressure at base of model
p_o	free-stream static pressure
q	dynamic pressure $\left(\frac{1}{2}\rho V^2\right)$
R	Reynolds number, based on $\bar{c}$
r	fuselage radius at station x
S	wing area
V	free-stream velocity
x	longitudinal distance from nose of body
α	angle of attack
ϵ	angle of downwash
ρ	free-stream density

All dimensions, forces, moments, pressures, densities, and velocities, are measured in the absolute English system of units where the slug is the unit of mass, the foot the unit of length, and the second the unit of time unless otherwise specifically noted. All angles are measured in degrees.

APPARATUS AND METHODS

Tunnel

This investigation was conducted in the Langley 8-foot high-speed tunnel which is a single-return, closed-throat tunnel with the low-speed return passage open to atmospheric pressure. A plaster liner installed in the tunnel formed the subsonic test section at the geometric minimum and extended downstream to form the supersonic test section (fig. 1). The subsonic test section had a constant Mach number distribution within 0.003 up to Mach numbers exceeding 0.96. In the supersonic test section,

[redacted]

the maximum Mach number deviation from the design Mach number of 1.2 was 0.02 (reference 3).

Model and Support

The subject configuration employed a wing with quarter-chord line swept back 35°, an aspect ratio of 4, a taper ratio of 0.6, and an NACA 65A006 airfoil section measured parallel to the plane of symmetry. The wing was mounted on a fuselage body of revolution of fineness ratio 10 achieved by cutting off the rear one sixth of a basic body of fineness ratio 12 (table I). The longitudinal position of the wing was such that the quarter-chord point of the mean aerodynamic chord coincided with the station of maximum body diameter (fig. 2). The surface of the model was maintained in a smooth condition throughout the investigation.

The wing was of composite construction consisting of an SAE 4130-steel core and a tin-bismuth shell (fig. 3). The fuselage was a hollow shell constructed of steel. An electrical strain-gage type of balance was contained within the fuselage and secured to the fuselage at its forward end. The rear portion of the balance comprised a sting for supporting the model in the center of the tunnel (reference 1). The sting was secured to a variable angle-of-attack mechanism controllable from outside the tunnel (fig. 1).

Tests and Measurements

The investigation was conducted through a subsonic Mach number range from 0.6 to 0.96 and at a Mach number of 1.2. The angle-of-attack range for the investigation was from -2° to 14° or from -2° to the angle of attack at which maximum allowable load on the balance was obtained.

The variation of test Reynolds number, based on the mean aerodynamic chord, was from approximately 1.73×10^6 at a Mach number of 0.6 to 2.02×10^6 at a Mach number of 0.96. At a Mach number of 1.2, the Reynolds number was 1.94×10^6 (fig. 4).

During subsonic testing, static pressures were observed along the tunnel wall in the region of the model location to insure that no data were affected by tunnel choking. For testing at a Mach number of 1.2 shadow images were used to show the position of the tunnel normal shock wave to insure its being to the rear of the model. No data presented herein are affected by these phenomena.

Measurements of lift, drag, and pitching moment about the 25-percent mean-aerodynamic-chord point were obtained from the internal balance system. Consideration of the accuracy of the strain-gage measurements

indicated the lift, drag, and pitching-moment coefficients to be approximately within ±0.01, ±0.001, and ±0.005, respectively, through the Mach number range.

Wake characteristics and downwash angles were obtained at each test point at a distance 1.225 semispans behind the 25-percent mean-aerodynamic-chord point for two spanwise locations at various distances above the wing-chord plane by means of two calibrated rakes. These rakes for the simultaneous measurement of wake profiles and downwash angles were affixed to the sting ahead of the angle-of-attack pivot so that the rakes maintained a constant position relative to the model. Details of the rake location with respect to the model are shown in figure 5. A photograph of the model showing the rakes in position is presented in figure 6.

Consideration of possible small errors in calibration, angle-of-attack measurement, scatter of test points, and variations in local static pressure indicated the accuracy of the measured downwash angles to be within $\pm 0.2^\circ$ for measurements made outside the wake and within $\pm 0.3^\circ$ for measurements made in the wake.

The static pressure at the rear of the model was obtained from a pressure orifice located on the side of the sting support in the plane of the model base.

Measurement of the angle of attack within 0.1° was accomplished by means of an optical device utilizing a system of reflected light beams. A description of the device can be found in reference 1.

Corrections

Expressions for evaluating the effects of model and wake blockage on Mach number and dynamic pressure and the effect of the pressure gradient caused by the wake on the drag coefficient were determined by utilizing an adaptation of the method of reference 4. Details of the method of application of these expressions are presented in reference 1. The expressions for the effects of the jet-boundary-induced upwash on angle of attack and angle of downwash were obtained from reference 5. The effects of compressibility were considered in all cases.

Evaluation of these effects indicated an appreciable correction to Mach number at subsonic Mach numbers of 0.85 and above which reached a magnitude of 1.4 percent at a Mach number of 0.96. Corrections to measured downwash angles were appreciable at all subsonic Mach numbers for lift coefficients of 0.3 and above and reached a maximum value of 0.2°. These corrections have been applied to the data. All other errors caused by blockage and boundary-induced upwash were negligible and corrections have not been applied to the data.

[redacted]

No specific tests were made to evaluate the interference effects of the sting support. Results of a previous investigation at low angles of attack (reference 6) indicated that, with no horizontal tail, the lift and pitching-moment tares were probably negligible. When the drag tare data of reference 6 was interpolated for the present configuration, it was estimated that the effect of the sting would be a decrease in drag coefficient of 0.003 at subsonic speeds and 0.002 at a Mach number of 1.2. Because of the uncertainty of these corrections at high angles of attack, no application to the data with the exception of the wing-fuselage drag at zero lift and the wing-fuselage lift-to-drag ratio has been made.

The presence of the sting probably resulted in an increase in the base pressures. Previous results (reference 6) indicated that the presence of the sting caused an increase in base-pressure coefficient of about 0.1 at all Mach numbers. These data also indicated that the presence of the sting would cause a decrease in downwash angle from approximately 1° at subsonic speeds to 0.2° at a Mach number of 1.2.

Measurements of total pressure in the wake have been corrected for the presence of a bow wave when it was present.

An analysis of the effects of the wing bending due to aerodynamic load was made by use of the methods of references 7 and 8 to determine the subcritical span load distribution. When the elastic axis is assumed to be at the 40-percent-chord line and any torsion about the elastic axis is neglected, static bending tests determined that these effects could be predicted by assuming that the bending occurs normal to the elastic axis and outboard of the 16-percent semispan station. Results indicated an average decrease in lift-curve slope of about 2 percent and a forward shift in aerodynamic center of 1.44 percent of the mean aerodynamic chord caused by the effective twist accompanying wing bending. A representative plot showing these effects for a subcritical Mach number is presented in figure 7. Corrections for these effects have not been applied since supercritical span load distributions could not be determined.

RESULTS AND DISCUSSION

The basic configuration of this investigation was the wing-fuselage combination. Data for the wing and wing-fuselage interference were obtained by subtracting data for the basic fuselage from corresponding data for the wing-fuselage combination. An estimation of the magnitude of the wing-fuselage interference effects from present data was considered to be impractical. No basic fuselage data are presented herein. These data may be found in reference 1.

[redacted]

The results of this investigation are presented in the following figures:

Force and moment characteristics:
C_L, C_D, C_m plotted against M for
wing fuselage 8
P_b plotted against M for
wing fuselage 9
α, C_D, C_m plotted against C_L for -
Wing fuselage 10
Wing and wing-fuselage interference 11
Summary . . . . . 12 through 15

Wake and downwash characteristics:
$\Delta H/q$ plotted against location for
wing fuselage 16
ϵ plotted against α for -
Wing fuselage 17
Wing and wing-fuselage interference 17
$\partial\epsilon/\partial\alpha$ plotted against M for -
Wing fuselage 18
Wing and wing-fuselage interference 18

Force and Moment Characteristics

Near zero lift the lift-curve slope for the wing-fuselage configuration was 0.06 at a Mach number of 0.6 (fig. 12) and was comparable to a low-speed value of 0.061 obtained for a similar, isolated wing in the Langley two-dimensional low-turbulence pressure tunnel (reference 9). This value increased with Mach number and reached a maximum of 0.085 at a Mach number of 0.93 followed by a decrease to 0.069 at a Mach number of 1.2.

The increase in lift-curve slope in the subcritical speed range is in agreement with the Prandtl-Glauert approximation for a compressible flow. The decrease in lift-curve slope above a Mach number of 0.93 can be attributed to the presence of shock and the accompanying separation over the wing.

At a lift coefficient of 0.4, the lift-curve slope exhibited characteristics similar to that at a lift coefficient of zero. The magnitude, however, was approximately 17 percent higher than that at a lift coefficient of zero probably because of an increase in effective camber caused by the formation of a region of separated flow near the leading edge (reference 9). The maximum lift-curve slope was reached at a Mach number approximately 0.02 lower than at a lift coefficient

of zero. It should be remembered, however, that the maximum Reynolds number of these tests was approximately 2×10^6; therefore, the characteristics just described could be altered at higher Reynolds numbers. An increase in Reynolds number would probably reduce the changes in lift-curve slope at the moderate angles of attack of this investigation.

At zero lift the drag coefficient for the wing-fuselage configuration remained constant at a value of 0.01 up to a Mach number of about 0.90 at which point the drag rise occurred (fig. 13). At a Mach number of 1.2 the drag coefficient was 0.028. These values have been corrected for the interference effects of the sting. The drag characteristics throughout the Mach number range for the wing and wing-fuselage interference, although approximately 36 percent lower, were similar to those of the wing-fuselage configuration. The values of drag coefficient for the wing and wing-fuselage interference are based on total wing area rather than exposed wing area and as a result are comparatively low.

Base-pressure coefficients were measured at the plane of the model base and are presented in figure 9.

A maximum lift-to-drag ratio of 15 for the wing-fuselage configuration was reached at a Mach number of 0.86 (fig. 14). Above this Mach number a rapid decrease in the ratio occurred. The drag values used in computing this ratio have been corrected for the interference effect of the sting. The uncertainty in the values of lift-drag ratio as a result of inaccuracies in the lift and drag measurements for the wing-fuselage configuration was estimated to range from ±8 percent at a Mach number of 0.6 to ±4 percent at a Mach number of 1.2.

At a lift coefficient of zero, the static-longitudinal-stability parameter $\frac{\partial C_m}{\partial C_L}$ for the wing-fuselage configuration remained essentially constant up to a Mach number of 0.85 with a rapid increase in stability indicated above this point (fig. 15). At low Mach numbers the aerodynamic center for the wing-fuselage configuration was located at 19 percent of the mean aerodynamic chord. At higher Mach numbers a rearward shift of aerodynamic center to 37 percent of the mean aerodynamic chord was indicated. For the wing and wing-fuselage interference the aerodynamic center at low Mach number was located at approximately 27 percent of the mean aerodynamic chord and at the high Mach numbers moved rearward to 47 percent of the mean aerodynamic chord. The presence of the fuselage caused a destabilizing tendency evidenced by a forward shift in aerodynamic center of about 8 percent of the mean aerodynamic chord.

As the lift coefficient was increased to 0.4, the characteristics of the wing-fuselage configuration were similar to those at a lift coefficient of zero but with an average rearward shift in aerodynamic center of 4 percent of the mean aerodynamic chord through the Mach number range.

[redacted]

For the wing and wing-fuselage interference this rearward shift had an average value of 2 percent of the mean aerodynamic chord. These results would indicate that a part of these rearward shifts in aerodynamic center could be attributed to the fuselage. These rearward shifts in aerodynamic-center location can also be attributed to the region of separated flow near the leading edge previously mentioned. This leading-edge separation decreases the magnitude of the leading-edge pressure peak while the chordwise extent of the decreased pressure increases. At Reynolds numbers higher than those of the present tests, however, the extent of the leading-edge separation may be altered such that the results presented herein may be affected.

Above an angle of attack of 10°, abrupt unstable movements in aerodynamic center were noted. These movements were more pronounced at higher Mach numbers (figs. 10(c) and 11(c)). This forward shift in aerodynamic center can be attributed to a complete separation of the flow over the tips.

Wake and Downwash Characteristics

A representative plot of the wake characteristics through the Mach number and angle-of-attack range tested at two spanwise locations at a distance 1.225 semispans behind the quarter-chord point of the mean aerodynamic chord is presented in figure 16. These data indicated that the wake would not extend beyond a point 0.25 semispan above the wing-chord plane for angles of attack of 8° or less. The increased intensity of the wake at the inboard location was probably caused by the presence of the fuselage (reference 1).

In figure 17 are presented the variations of downwash angle with angle of attack at a distance 1.225 semispans behind the 25-percent point of the mean aerodynamic chord. This variation is presented for two spanwise locations at various heights above the wing-chord plane. The downwash angle measured near the fuselage was very erratic at angles of attack above 4° for all Mach numbers at the 0.125 semispan location above the wing-chord plane. An examination of the wake-width data for the inboard location for the fuselage configuration (reference 1) indicated that these erratic variations can be attributed to the wake of the fuselage. Wake width and downwash data indicated that a horizontal tail located at the base of the model should not be located between 0.125 and 0.25 semispan above the wing-chord plane.

The data indicate that decreases in static longitudinal stability can be expected at all subsonic Mach numbers for angles of attack greater than about 7° for a configuration employing a horizontal tail. An important change in the angle of attack for zero downwash occurs between a Mach number of 0.96 and 1.2 (fig. 17(b)) for the wing-fuselage

combination as compared with the wing and wing-fuselage interference data. This shift in the angle of attack for zero downwash is attributed to the fuselage since no such change is indicated for the wing and wing-fuselage interference. As a consequence, important changes in trim of an airplane flying in this Mach number range can be expected from this shift.

Figure 18 presents the rate of change of downwash angle with angle of attack as a function of Mach number. The values presented are spanwise averages for a location 0.25 semispan above the wing-chord plane. At a lift coefficient of zero, the rate of change of downwash angle with angle of attack for the wing-fuselage configuration increased from a value of 0.435 at a Mach number of 0.6 to a maximum value of 0.58 at a Mach number of 0.91. At a Mach number of 1.2, the value decreased to 0.144. Wing and wing-fuselage interference results indicated a reduction in these values at subsonic Mach numbers by about 26 percent and an increase in the value at a Mach number of 1.2 by about 31 percent.

At a lift coefficient of 0.4, a rapid increase in the rate of change of downwash angle with angle of attack occurred above a Mach number of of 0.825. Above a Mach number of 0.875 a decrease in this value was indicated with a minimum value being reached at a Mach number of 1.2.

CONCLUSIONS

From an investigation of the aerodynamic characteristics of a wing-fuselage configuration employing a wing with quarter-chord line swept back 35°, an aspect ratio of 4, a taper ratio of 0.6, and an NACA 65A006 airfoil section, the following conclusions may be drawn:

1. The increase in lift-curve slope was approximately in accordance with the Prandtl-Glauert approximation up to a Mach number of 0.93 at which point a lift-force break occurred. The drag-force break occurred at a Mach number of approximately 0.9.

2. The static longitudinal stability of the configuration remained essentially constant in the low-lift-coefficient range to a Mach number of 0.85 above which a marked increase in stability occurred. At high angles of attack, abrupt destabilizing movements of the aerodynamic center occurred.

3. For a configuration employing a horizontal tail, decreases in static longitudinal stability can be expected at all subsonic speeds above an angle of attack of approximately 7°.

[redacted]

4. Between the Mach numbers of 0.96 and 1.2 changes in trim can be expected near zero lift because of the corresponding change in the character of the downwash.

5. A horizontal tail located at the rear of the configuration should not be placed between 0.125 and 0.25 semispan above the wing-chord plane because of the severity of the wake in this region.

6. In the low-lift-coefficient range the rate of change of downwash angle with angle of attack increased to a Mach number of 0.91 above which a decrease occurred.

Langley Aeronautical Laboratory
National Advisory Committee for Aeronautics
Langley Air Force Base, Va.

[redacted]

REFERENCES

1. Osborne, Robert S.: A Transonic-Wing Investigation in the Langley 8-Foot High-Speed Tunnel at High Subsonic Mach Numbers and at a Mach Number of 1.2. Wing-Fuselage Configuration Having a Wing of 45° Sweepback, Aspect Ratio 4, Taper Ratio 0.6, and NACA 65A006 Airfoil Section. NACA RM L50H08, 1950.

2. Donlan, Charles J., Myers, Boyd C., and Mattson, Axel T.: A Comparison of the Aerodynamic Characteristics at Transonic Speeds of Four Wing-Fuselage Configurations as Determined from Different Test Techniques. NACA RM L50H02, 1950.

3. Ritchie, Virgil S., Wright, Ray H., and Tulin, Marshall P.: An 8-Foot Axisymmetrical Fixed Nozzle for Subsonic Mach Numbers up to 0.99 and for a Supersonic Mach Number of 1.2. NACA RM L50A03a, 1950.

4. Herriot, John G.: Blockage Corrections for Three-Dimensional-Flow Closed-Throat Wind Tunnels, with Consideration of the Effect of Compressibility. NACA RM A7B28, 1947.

5. Eisenstadt, Bertram J.: Boundary-Induced Upwash for Yawed and Swept-back Wings in Closed Circular Wind Tunnels. NACA TN 1265, 1947.

6. Osborne, Robert S.: High-Speed Wind-Tunnel Investigation of the Longitudinal Stability and Control Characteristics of a $\frac{1}{16}$-Scale Model of the D-558-2 Research Airplane at High Subsonic Mach Numbers and at a Mach Number of 1.2. NACA RM L9C04, 1949.

7. De Young, John: Theoretical Additional Span Loading Characteristics of Wings with Arbitrary Sweep, Aspect Ratio, and Taper Ratio. NACA TN 1491, 1947.

8. Diederich, Franklin W.: A Simple Approximate Method for Obtaining Spanwise Lift Distributions over Swept Wings. NACA RM L7I07, 1948.

9. Cahill, Jones F., and Gottlieb, Stanley M.: Low-Speed Aerodynamic Characteristics of a Series of Swept Wings Having NACA 65A006 Airfoil Sections. NACA RM L50F16, 1950.

TABLE I

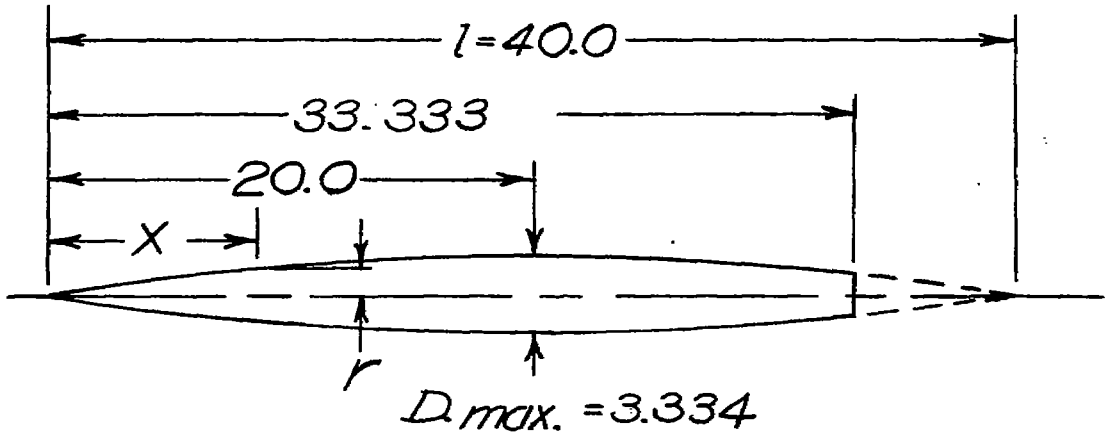

FUSELAGE ORDINATES			
x/l	r/l	x/l	r/l
0	0		
.0050	.00231	.4500	.04143
.0075	.00298	.5000	.04167
.0125	.00428	.5500	.04130
.0250	.00722	.6000	.04024
.0500	.01205	.6500	.03842
.0750	.01613	.7000	.03562
.1000	.01971	.7500	.03128
.1500	.02593	.8000	.02526
.2000	.03090	.8333	.02083
.2500	.03465	.8500	.01852
.3000	.03741	.9000	.01125
.3500	.03933	.9500	.00439
.4000	.04063	1.0000	0
L. E. radius = 0.0005			

NACA

All dimensions are in inches

[redacted]

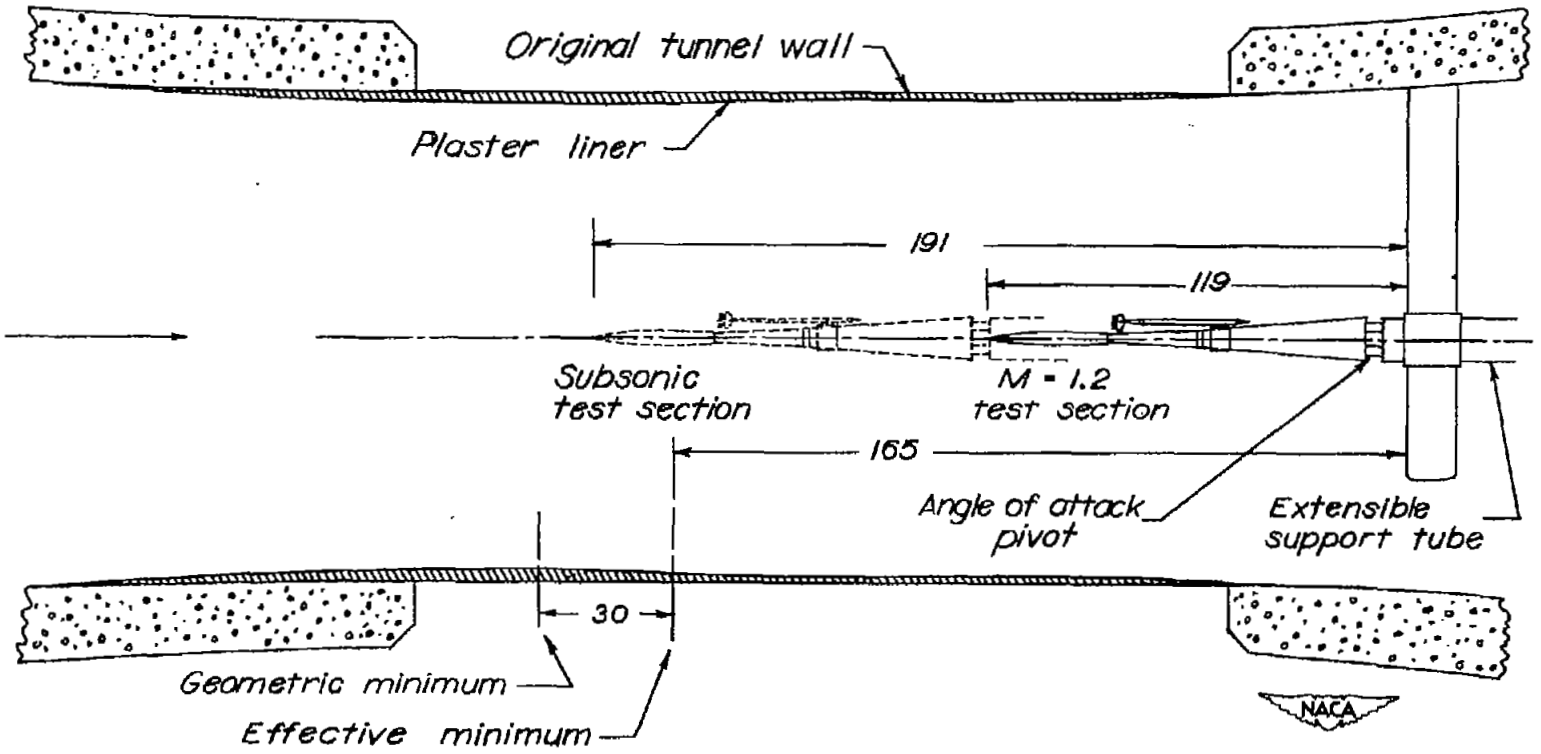

Figure 1.- Drawing of model locations in the subsonic and supersonic test sections of the Langley 8-foot high-speed tunnel. All dimensions are in inches.

Airfoil section (parallel to plane of symmetry)	NACA 65A006
Area, sq ft	1.0
Aspect ratio	4.0
Taper ratio	0.6
Incidence, deg	0.0
Dihedral, deg	0.0
Twist, deg	0.0

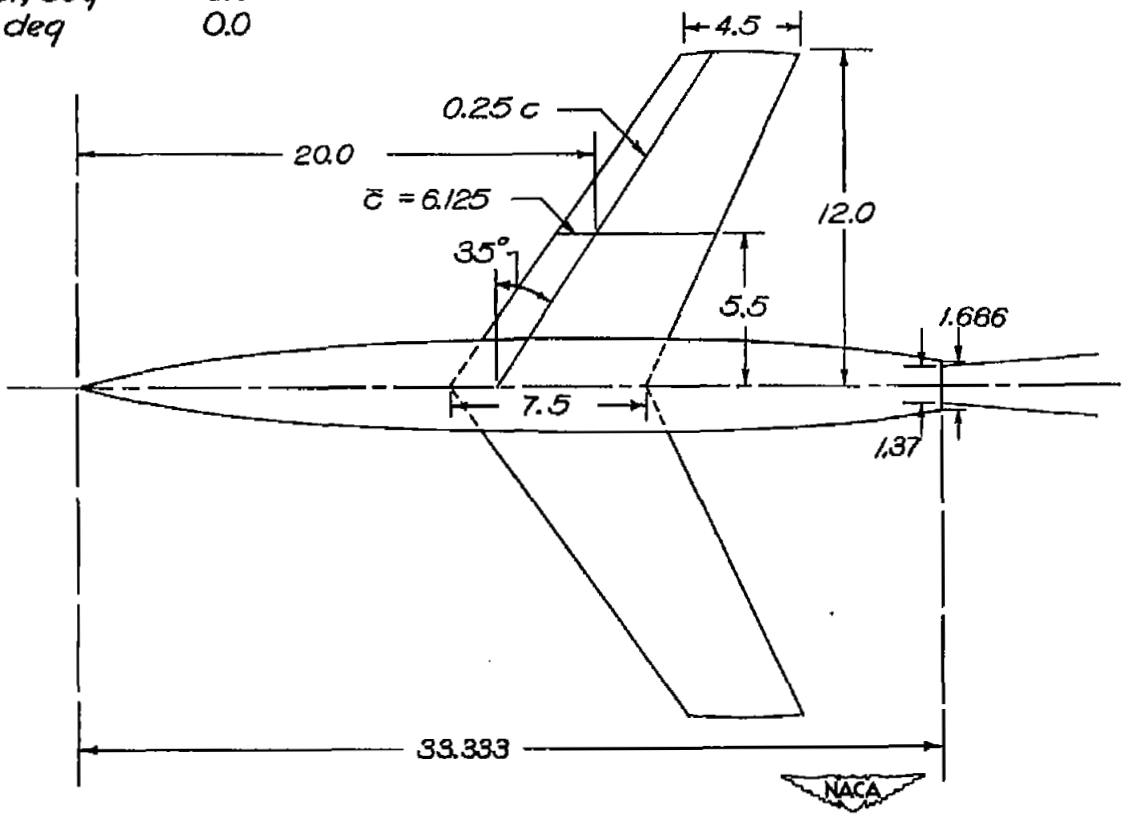

Figure 2.- Details of the test configuration employing a wing with quarter-chord line sweptback 35°, an aspect ratio of 4, a taper ratio of 0.6, and an NACA 65A006 airfoil section. All dimensions are in inches.

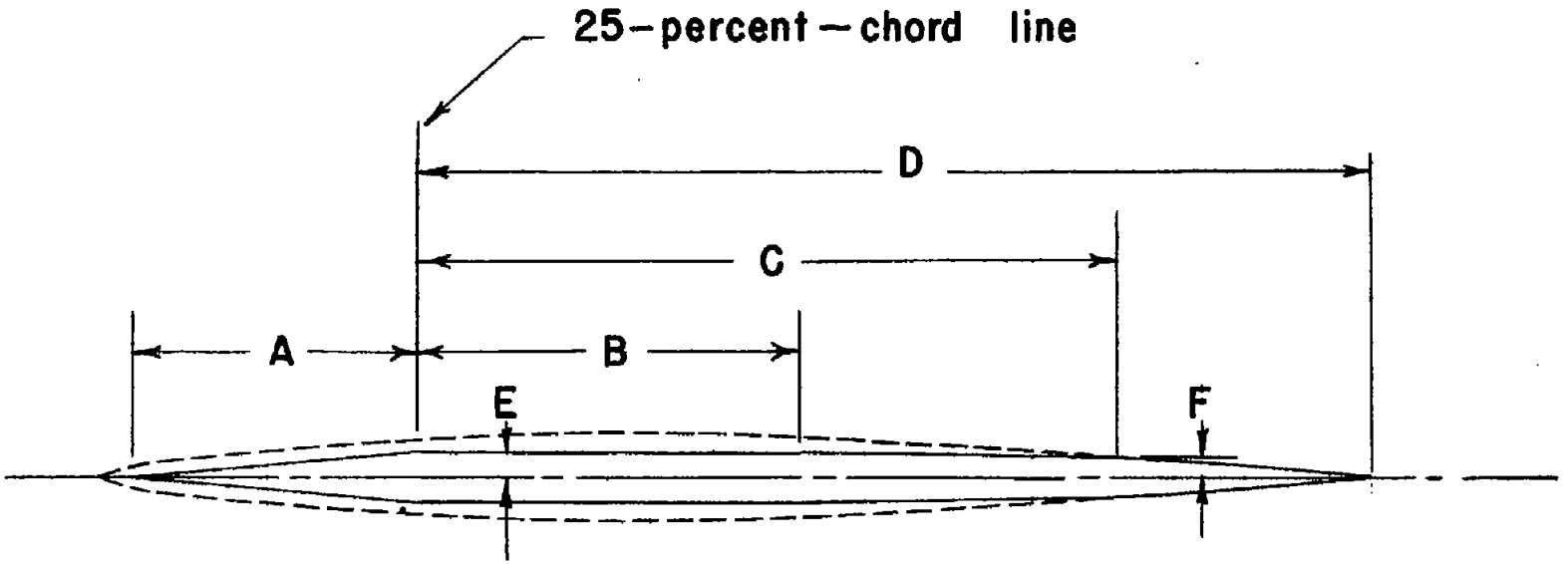

Section	A	B	C	D	E	F
Root	1.688	2.250	4.125	5.625	0.149	0.100
Tip	1.013	1.350	2.475	3.375	0.090	0.065

Figure 3.- Detail of wing construction showing the SAE 4130-steel core.

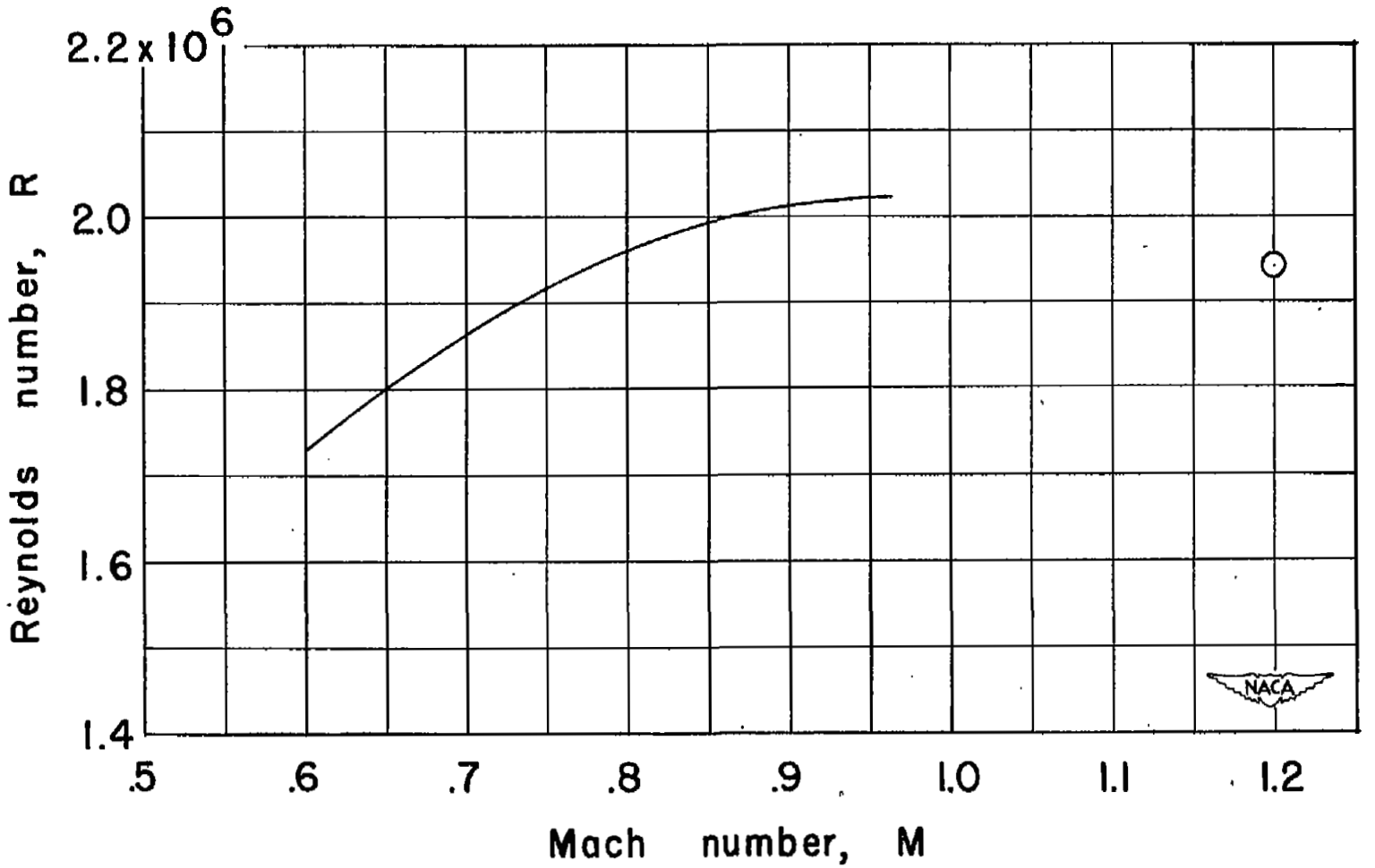

Figure 4.- Variation of test Reynolds numbers, based on a $\bar{c}$ of 0.51 foot, with Mach number.

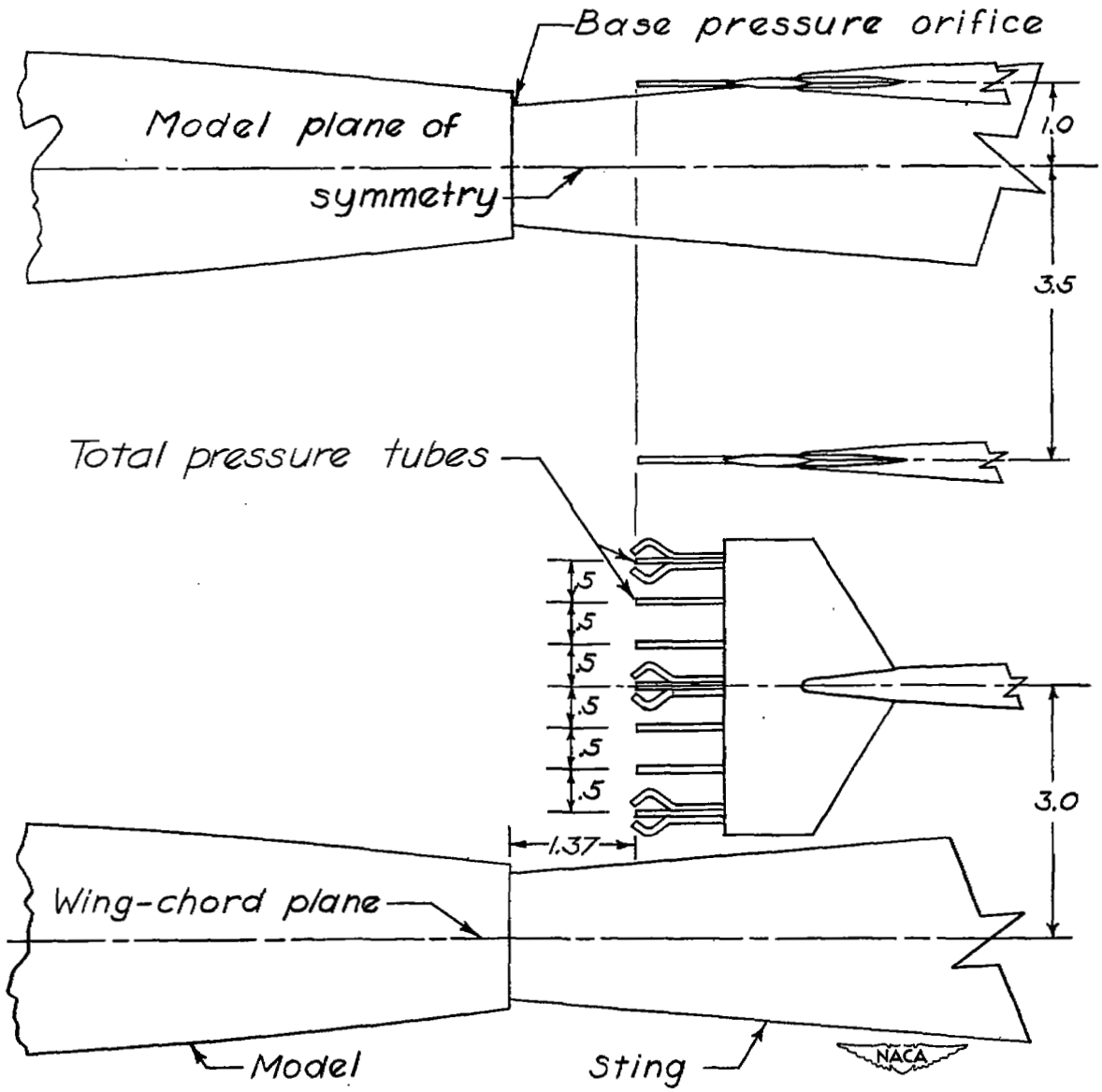

Figure 5.- Details of the rakes used for the wake survey and downwash measurements. All dimensions are in inches.

Figure 6.- Photograph of the model in the Langley 8-foot high-speed tunnel.

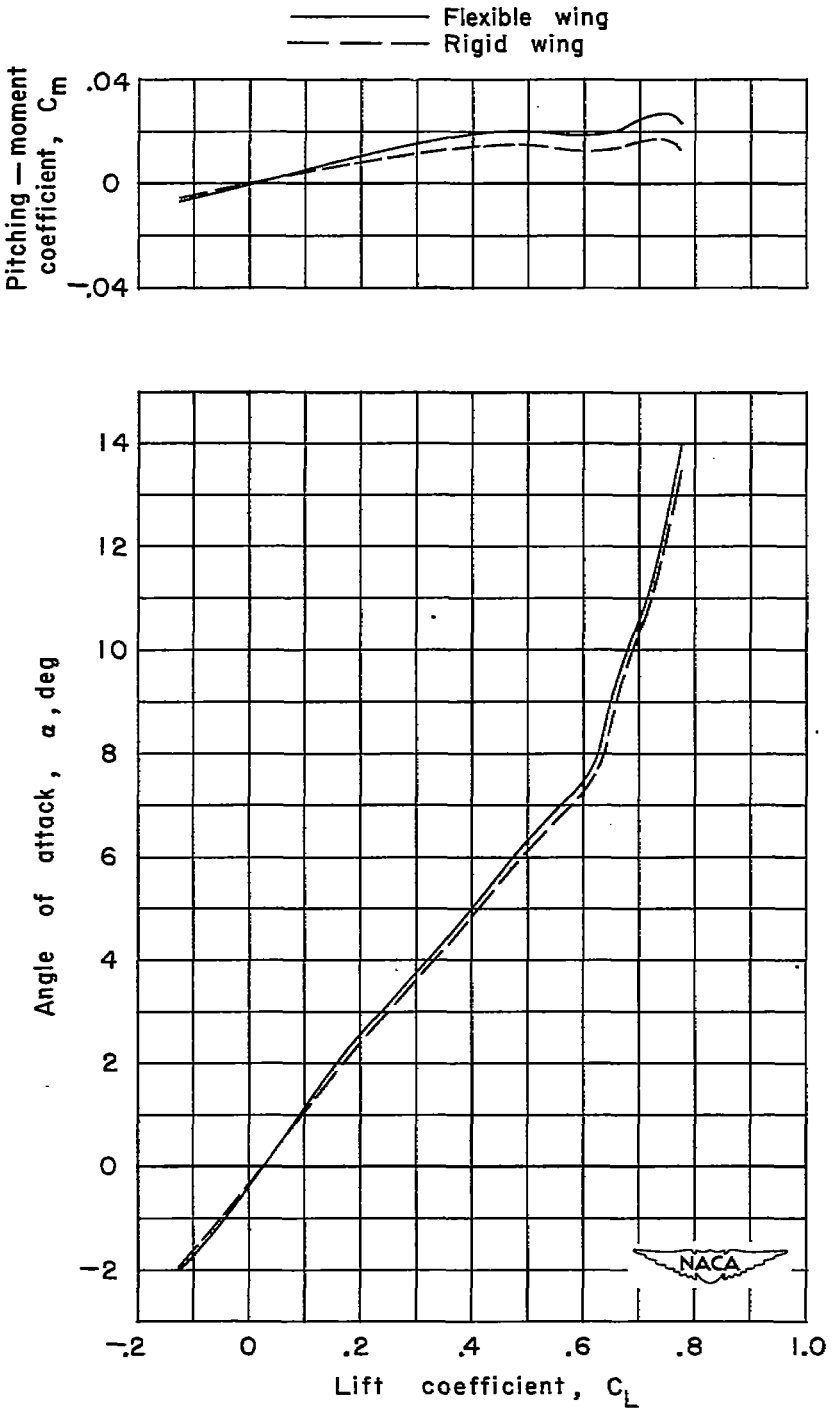

Figure 7.- Effect of the wing bending on angle of attack and pitching-moment coefficient for the wing-fuselage configuration at a Mach number of 0.8.

[redacted]

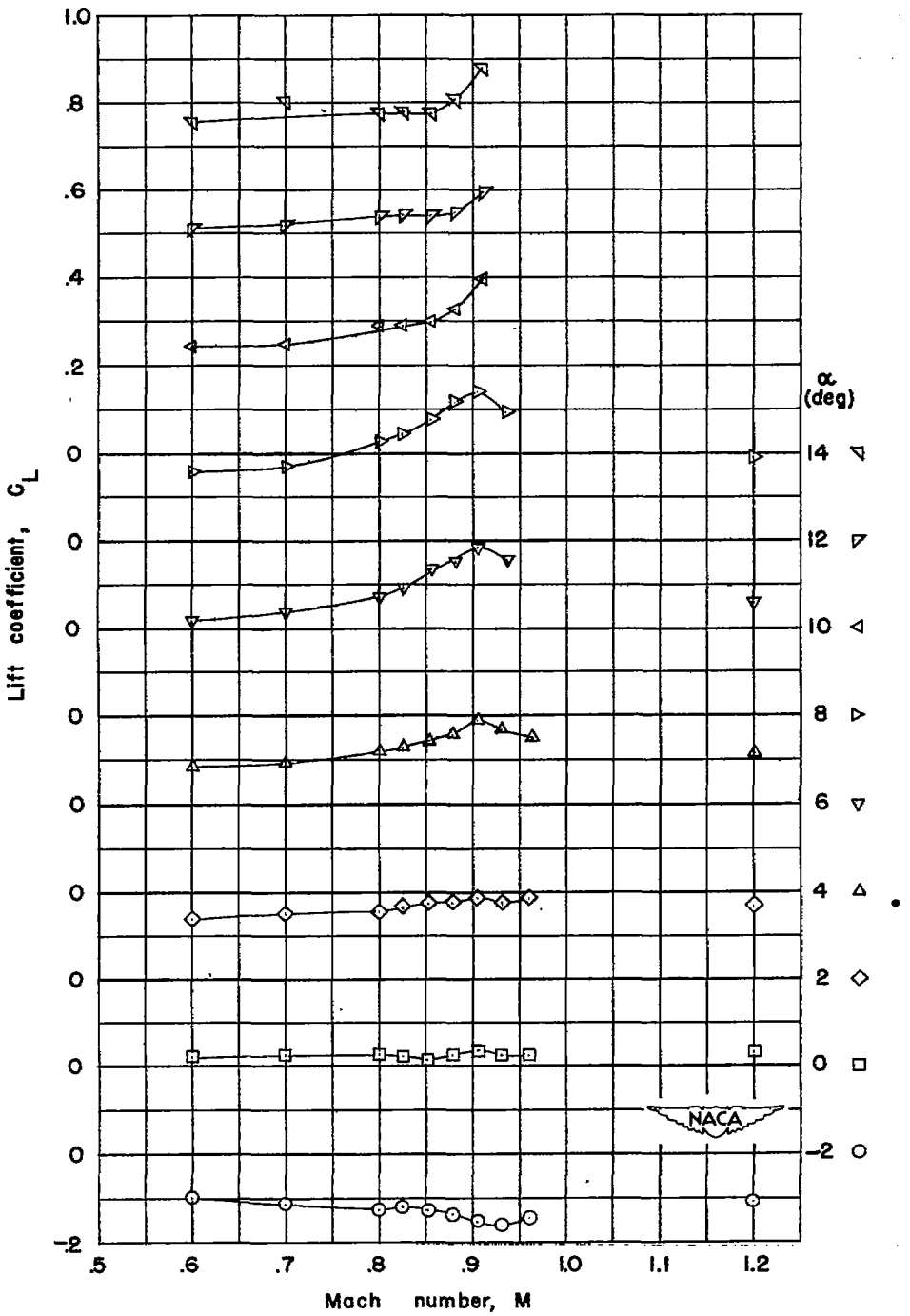

(a) Lift coefficient.

Figure 8.- Variation of the aerodynamic characteristics of the wing-fuselage configuration with Mach number.

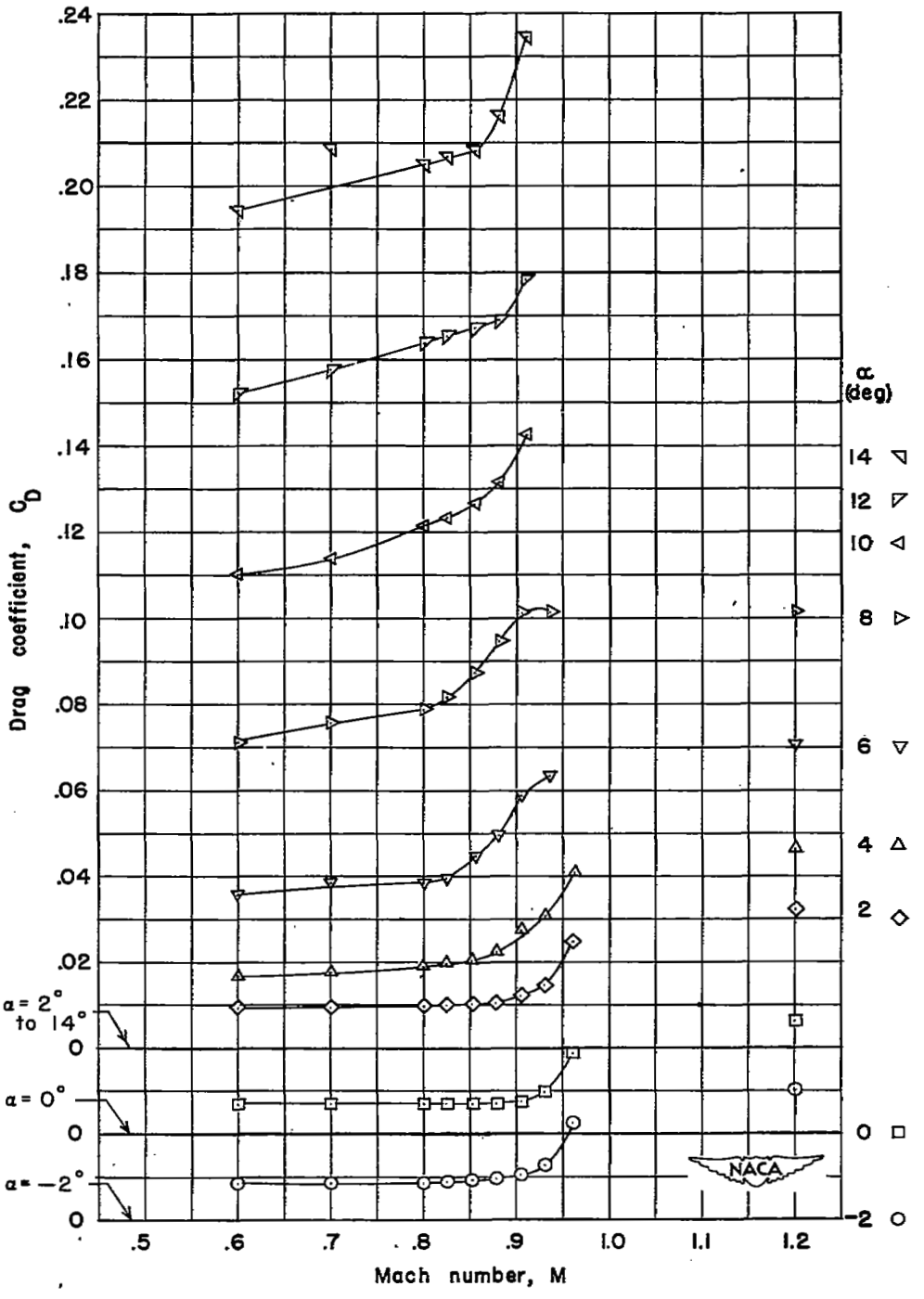

(b) Drag coefficient.

Figure 8.- Continued.

[redacted]

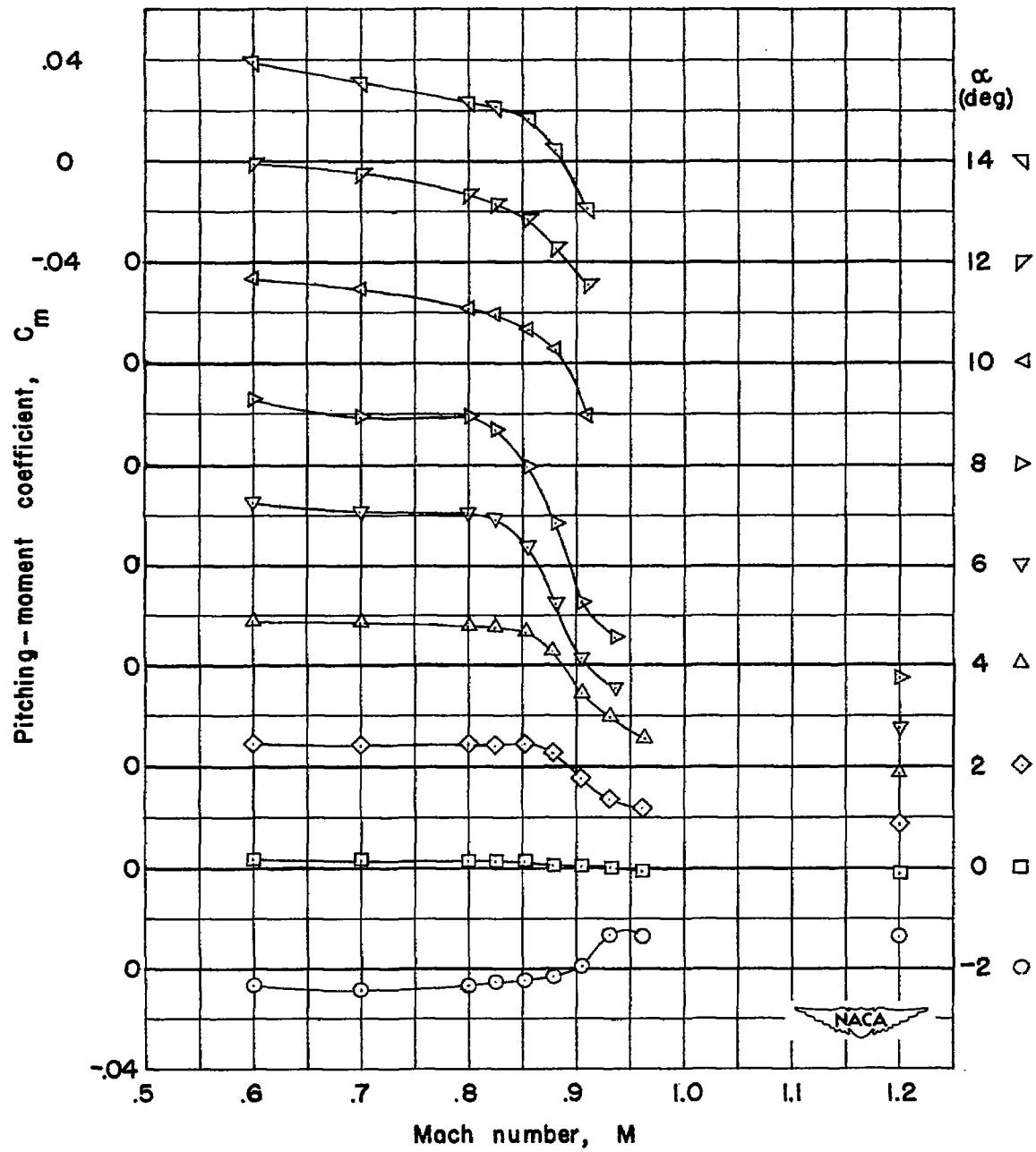

(c) Pitching-moment coefficient.

Figure 8.- Concluded.

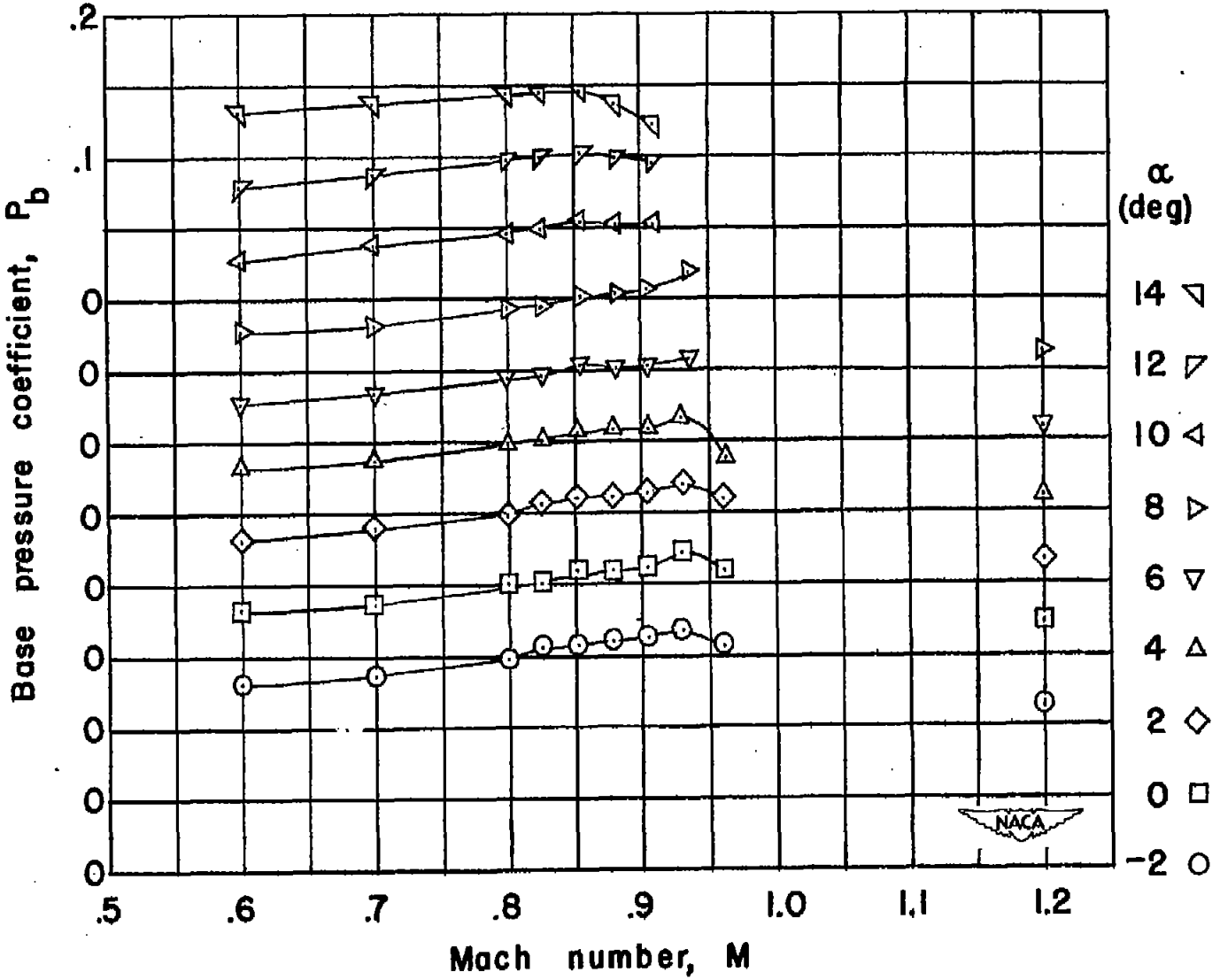

Figure 9.- Variation of base-pressure coefficient with Mach number for the wing-fuselage configuration.

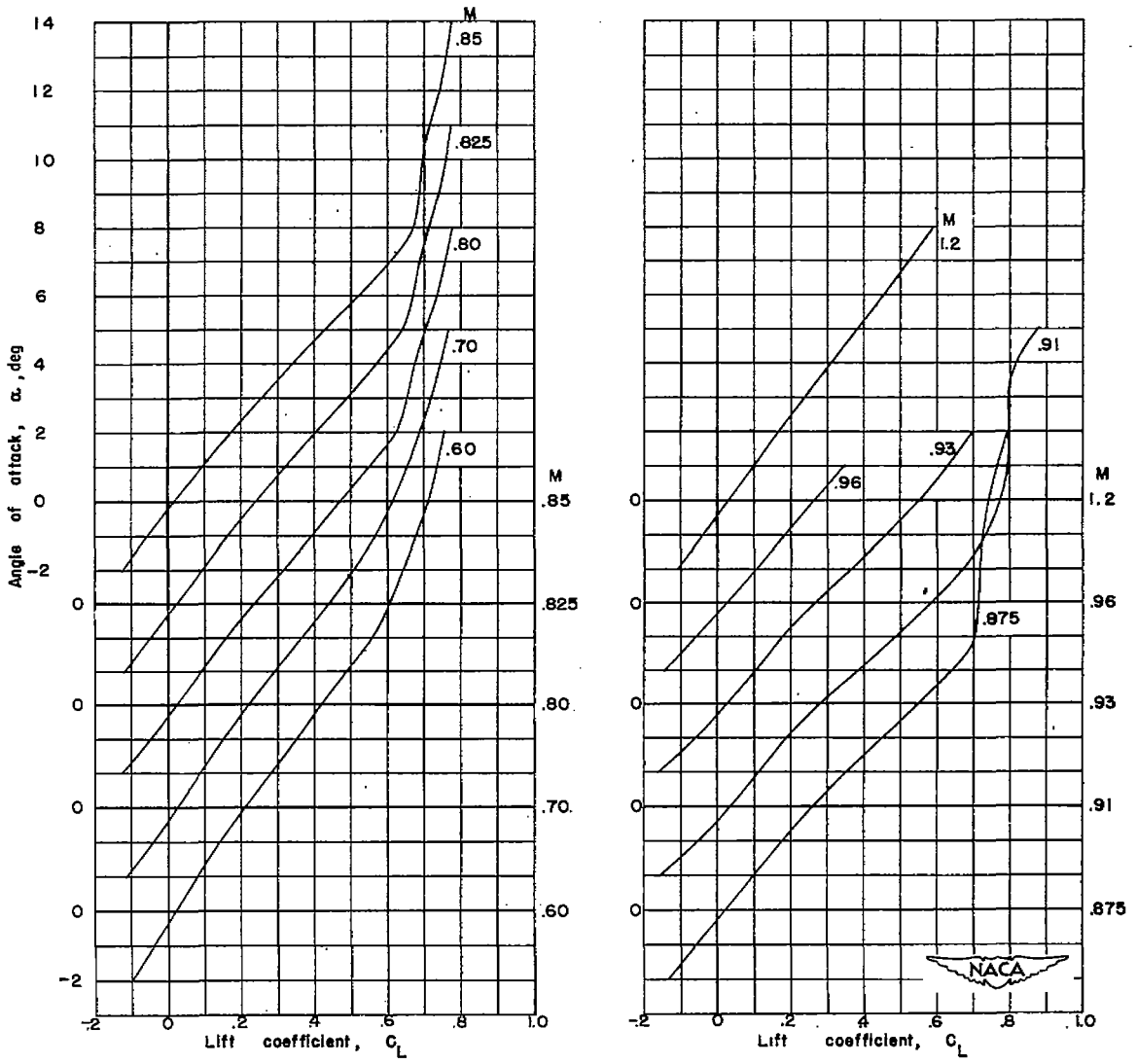

(a) Angle of attack.

Figure 10.- Variation of the aerodynamic characteristics of the wing-fuselage configuration with lift coefficient.

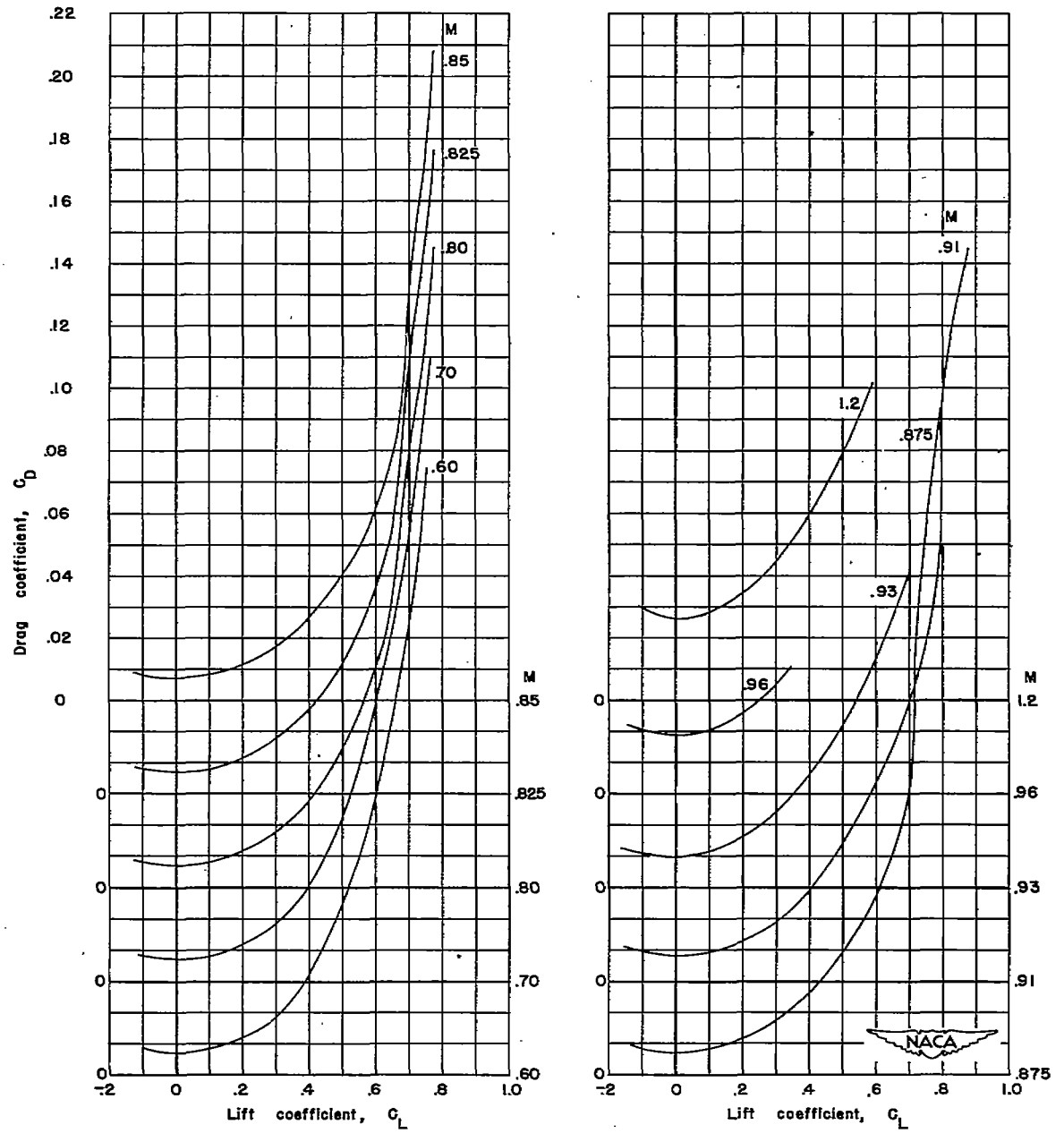

(b) Drag coefficient.

Figure 10.- Continued.

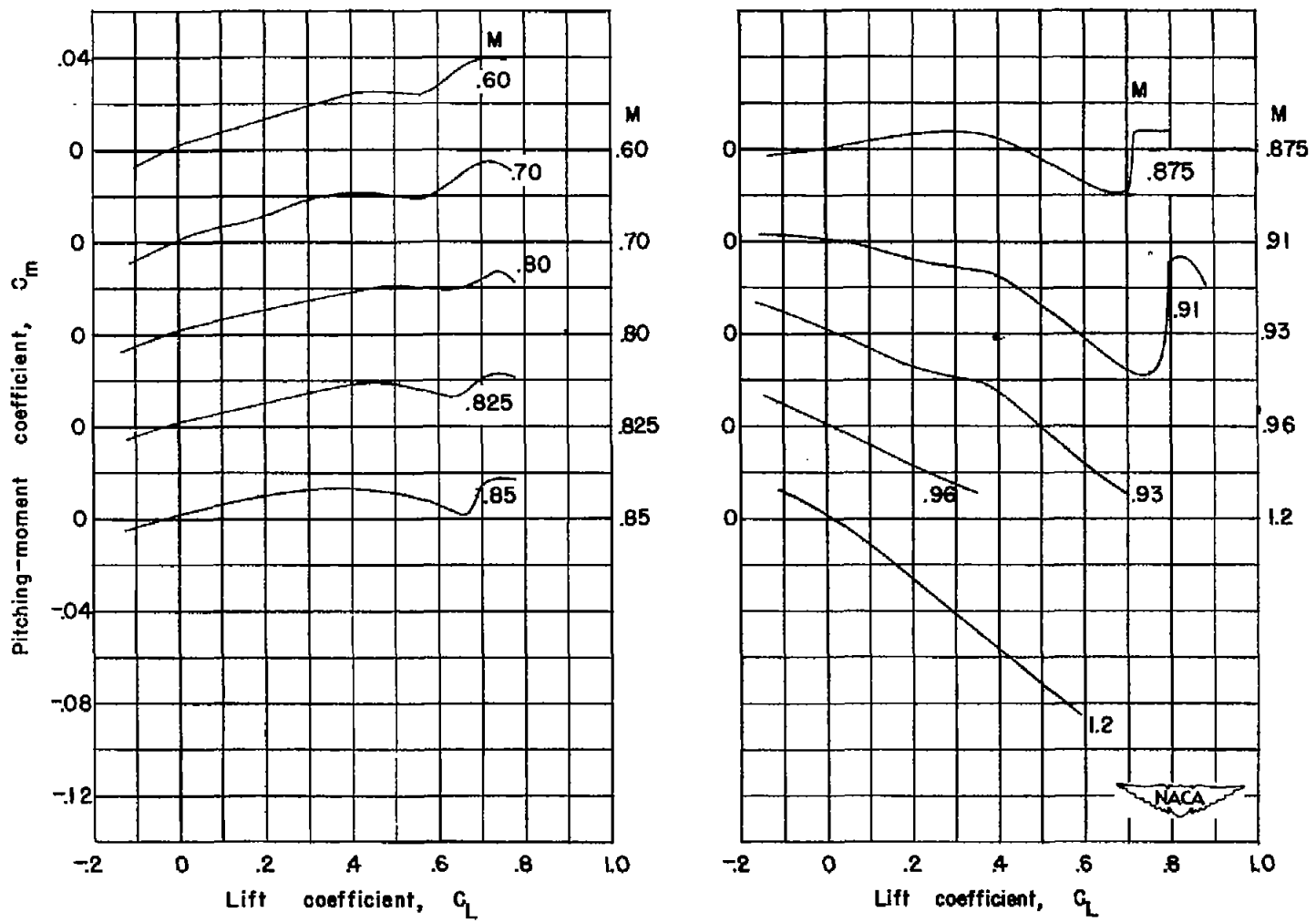

(c) Pitching-moment coefficient.

Figure 10.- Concluded.

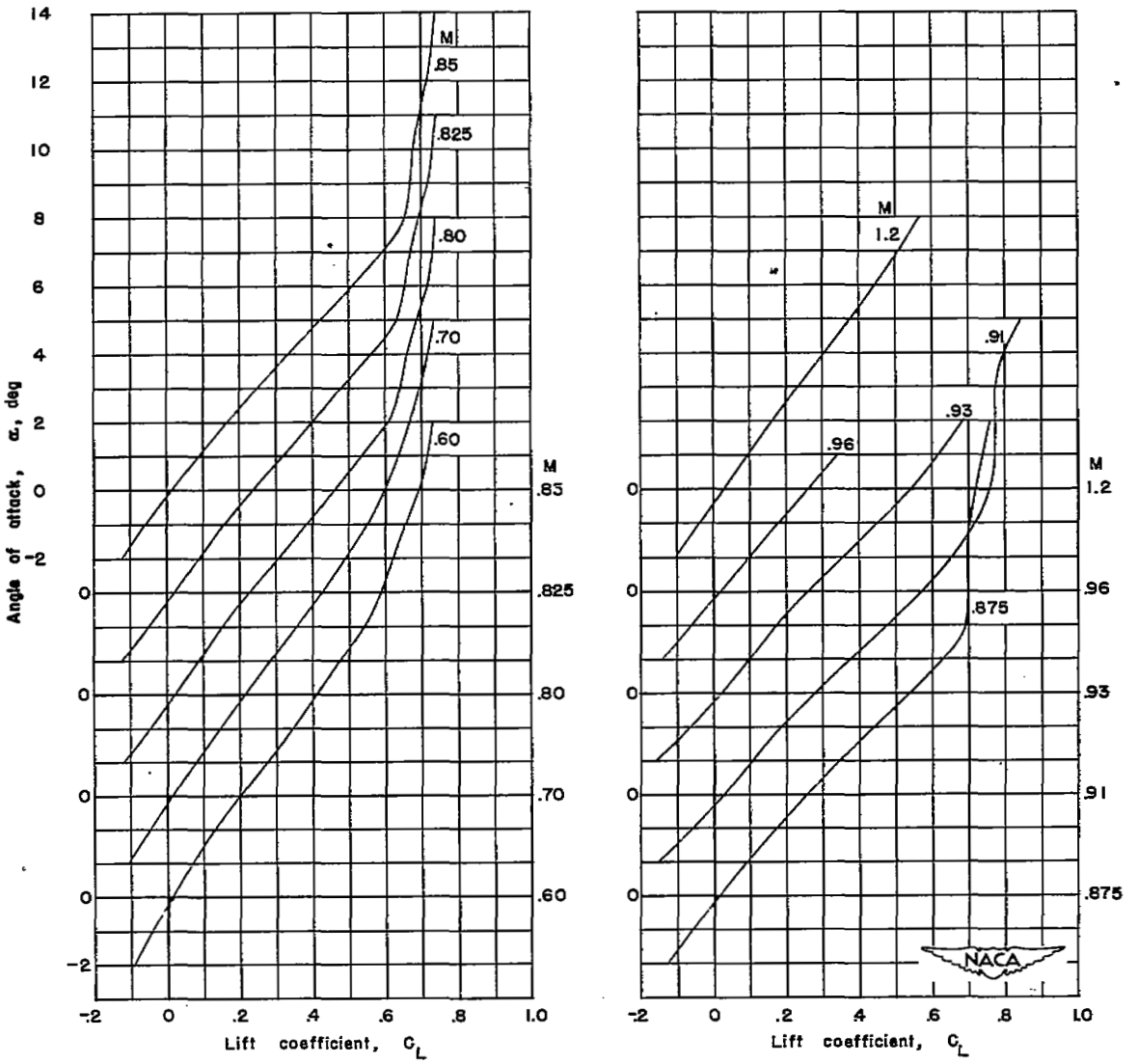

(a) Angle of attack.

Figure 11.- Variation of the aerodynamic characteristics of the wing and wing-fuselage interference with lift coefficient.

[redacted]

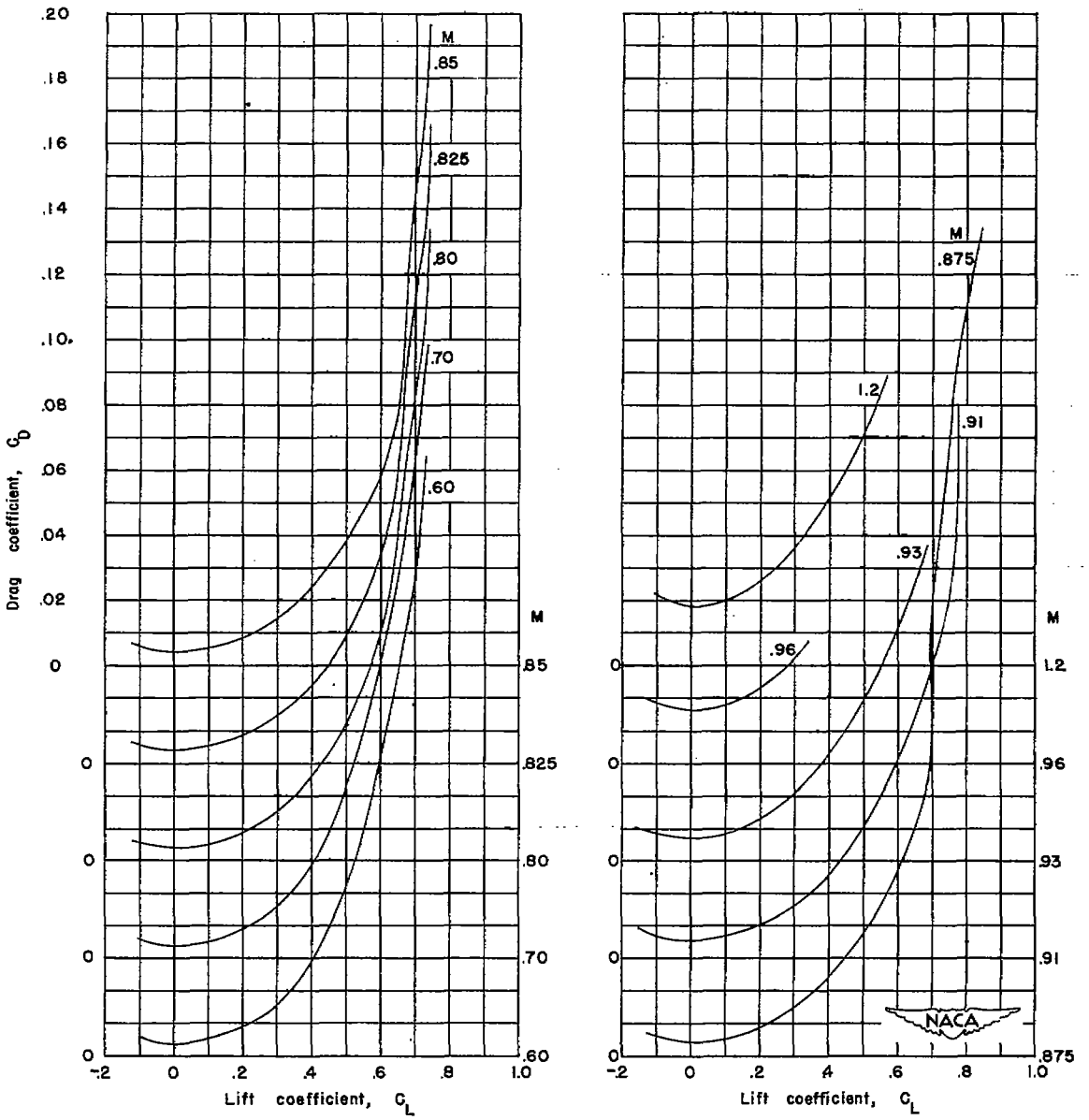

(b) Drag coefficient.

Figure 11.- Continued.

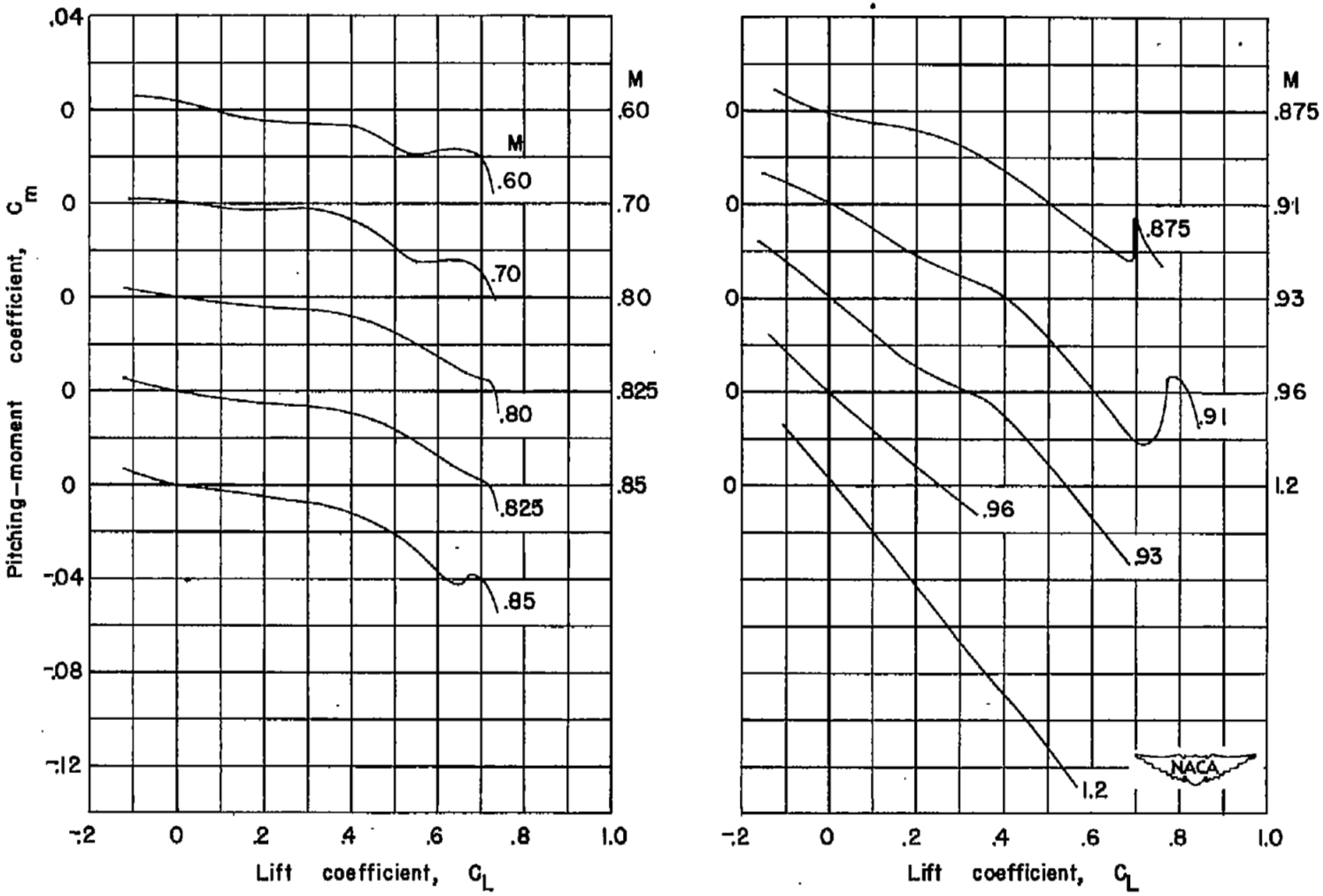

(c) Pitching-moment coefficient.

Figure 11.- Concluded.

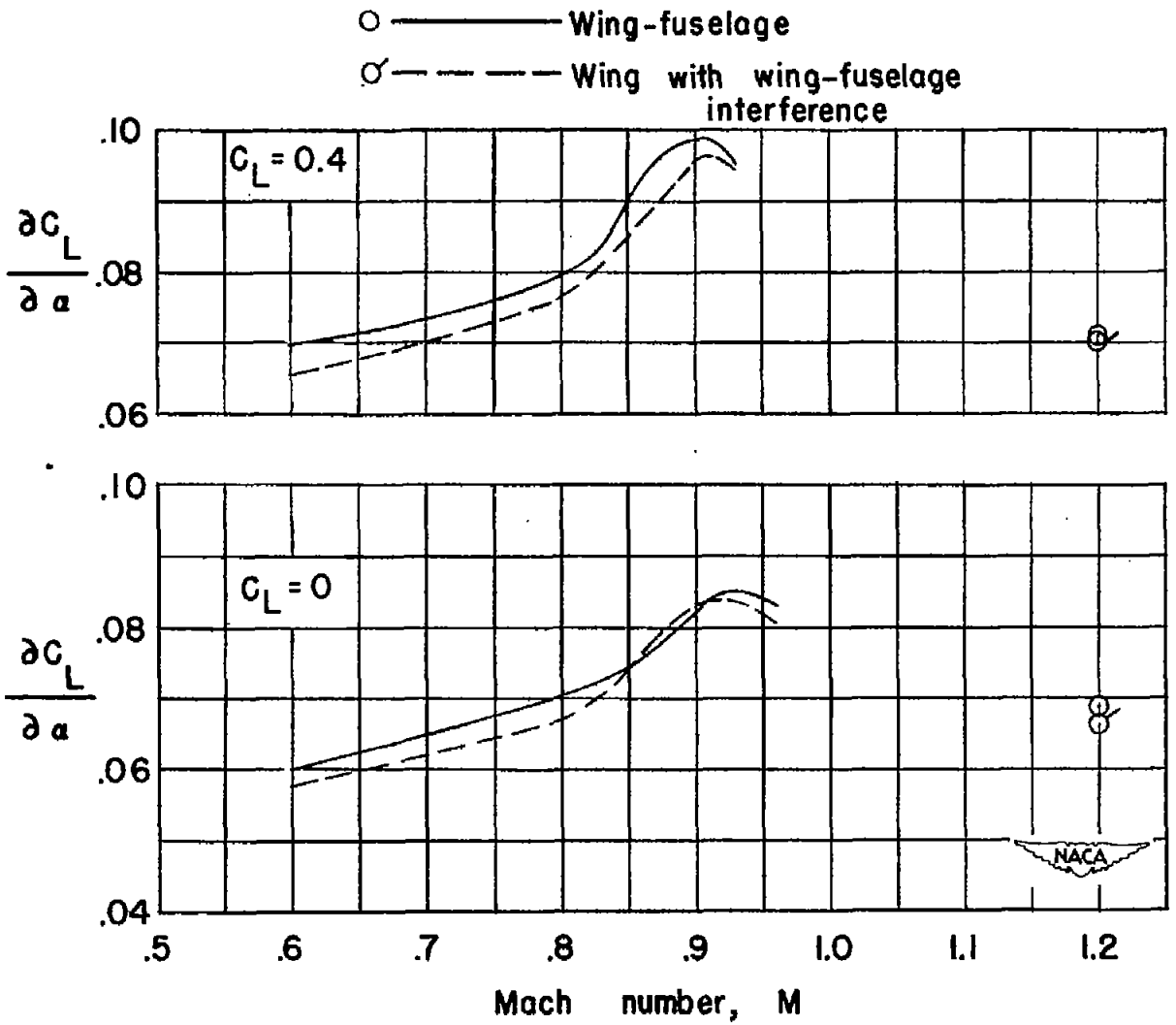

Figure 12.- Variation of lift-curve slope with Mach number for the wing-fuselage configuration and the wing with wing-fuselage interference.

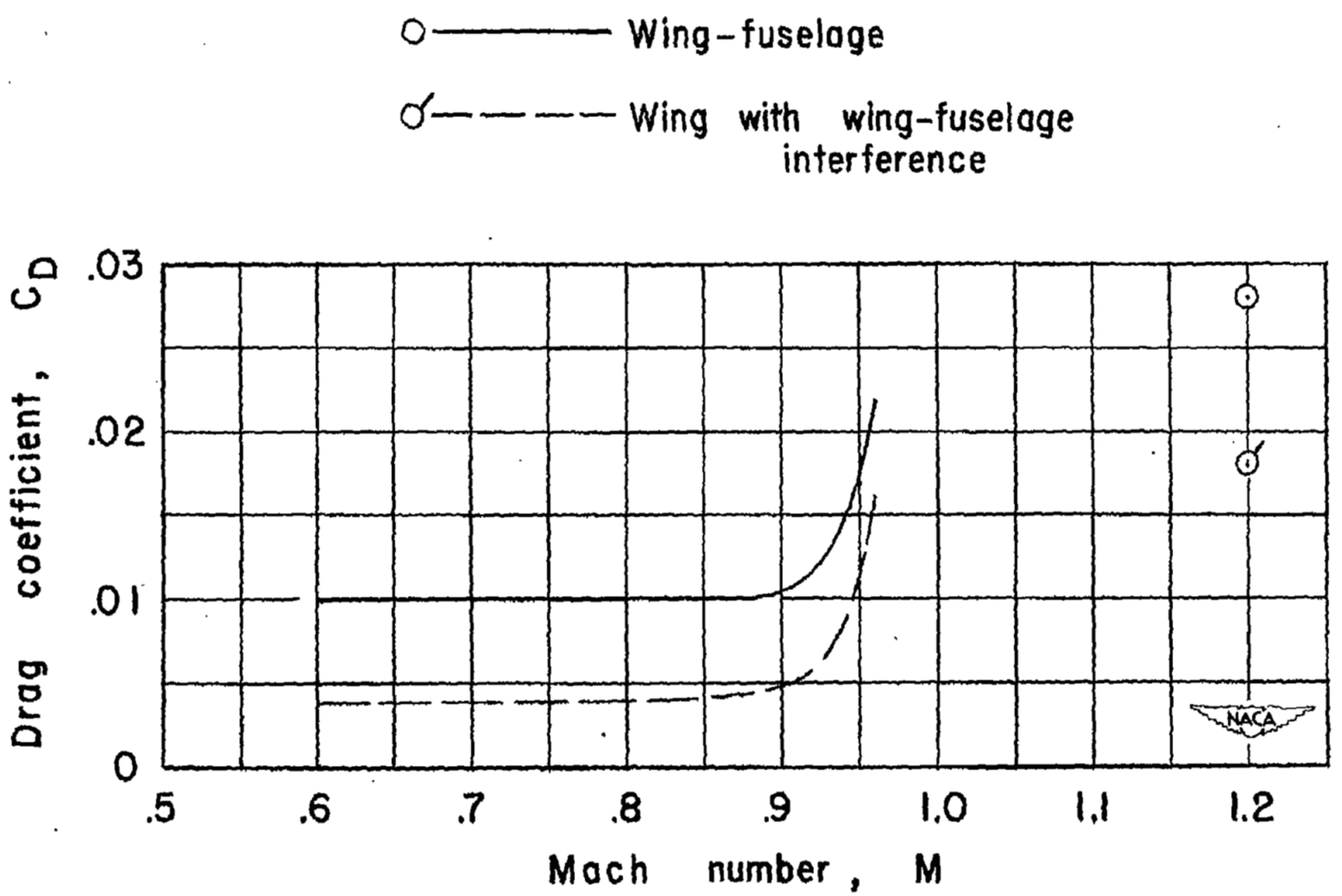

Figure 13.- Drag characteristics at zero lift as a function of Mach number for the wing-fuselage configuration and the wing with wing-fuselage interference.

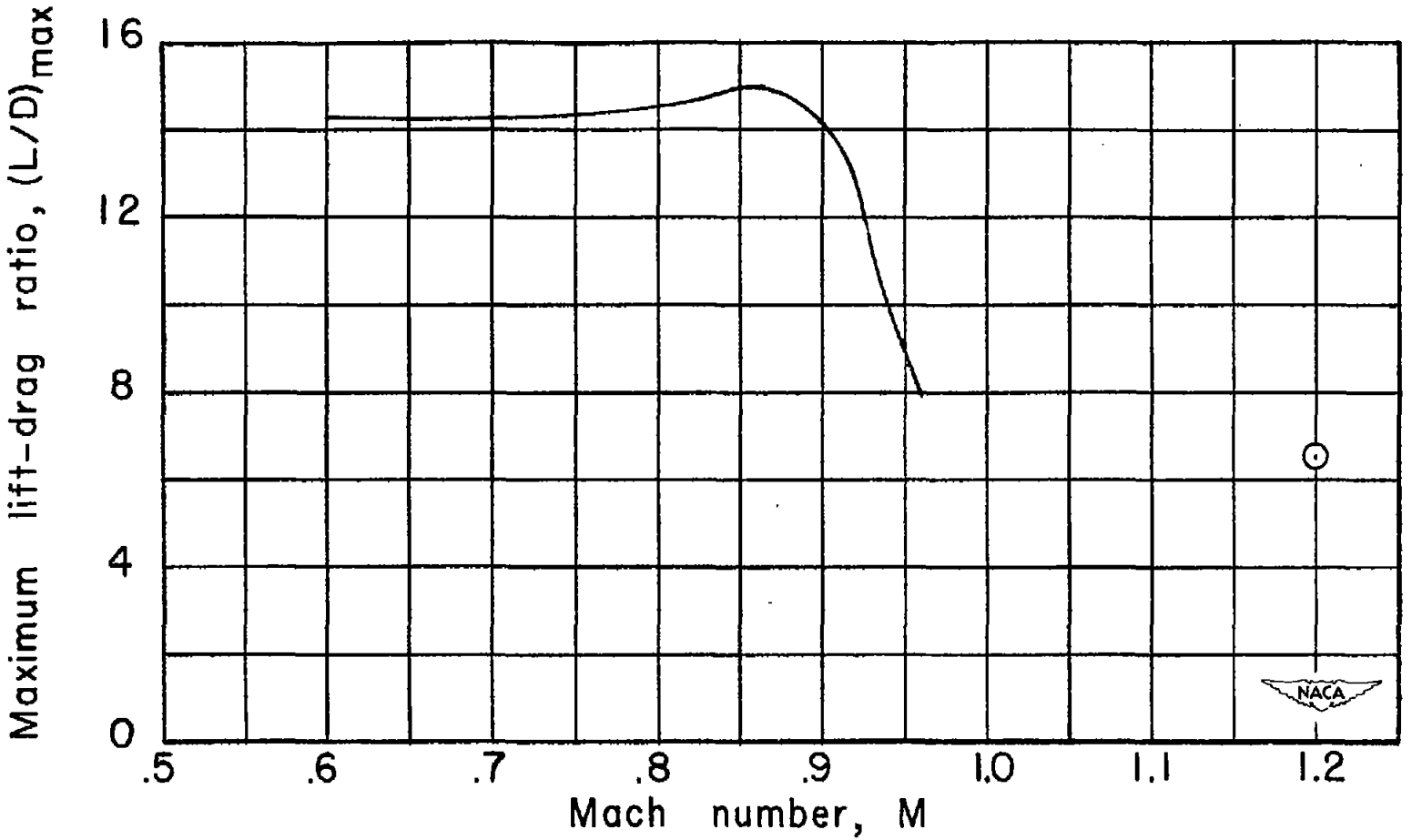

Figure 14.- Variation of maximum lift-to-drag ratio with Mach number for the wing-fuselage configuration.

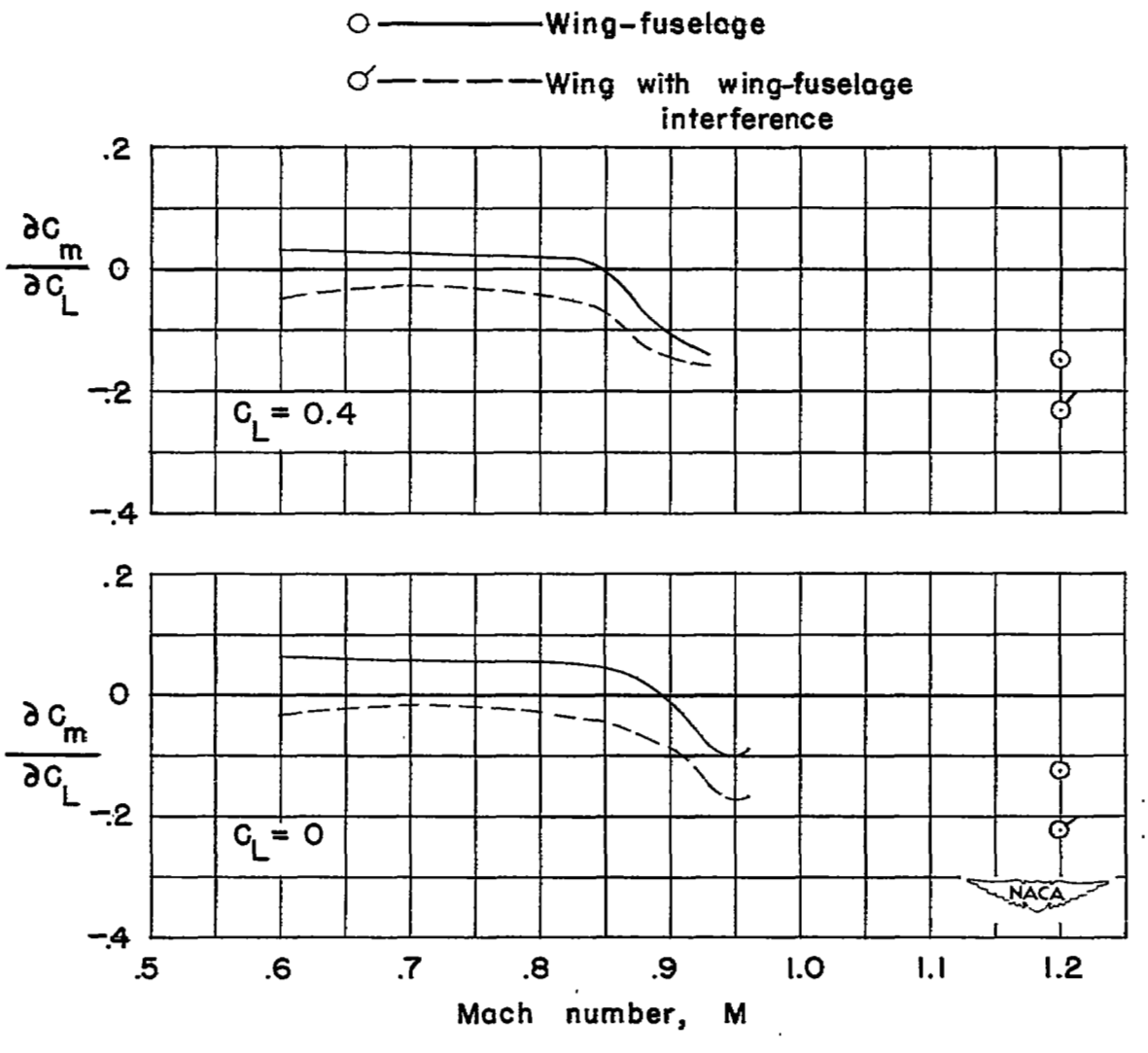

Figure 15.- Variation of the static-longitudinal-stability parameter, $\frac{\partial C_m}{\partial C_L}$, with Mach number for the wing-fuselage configuration and the wing with wing-fuselage interference.

[redacted]

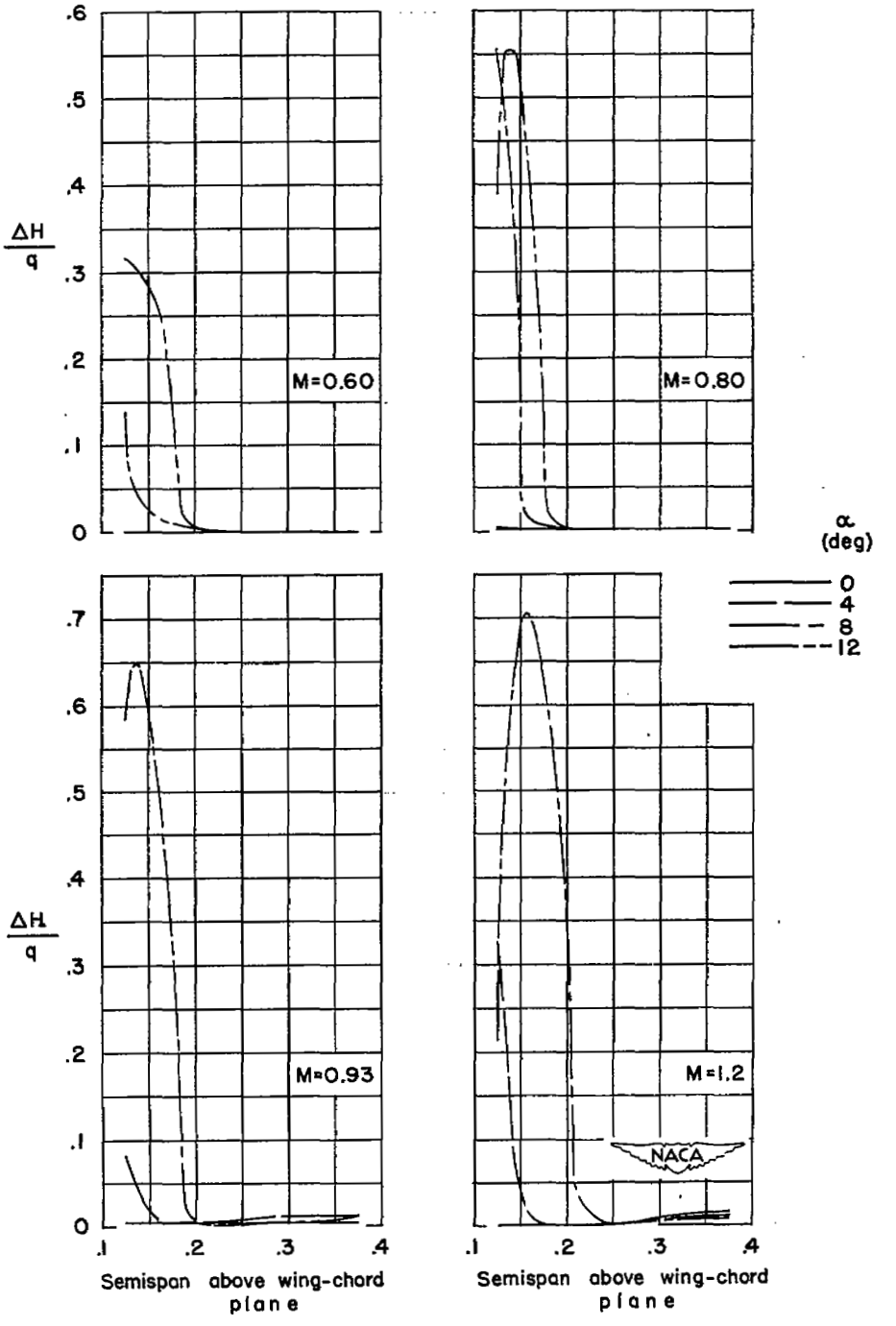

(a) 0.083 semispan from plane of symmetry.

Figure 16.- Wake characteristics at a point 1.225 semispans behind the wing 0.25$\bar{c}$ point for the wing-fuselage configuration.

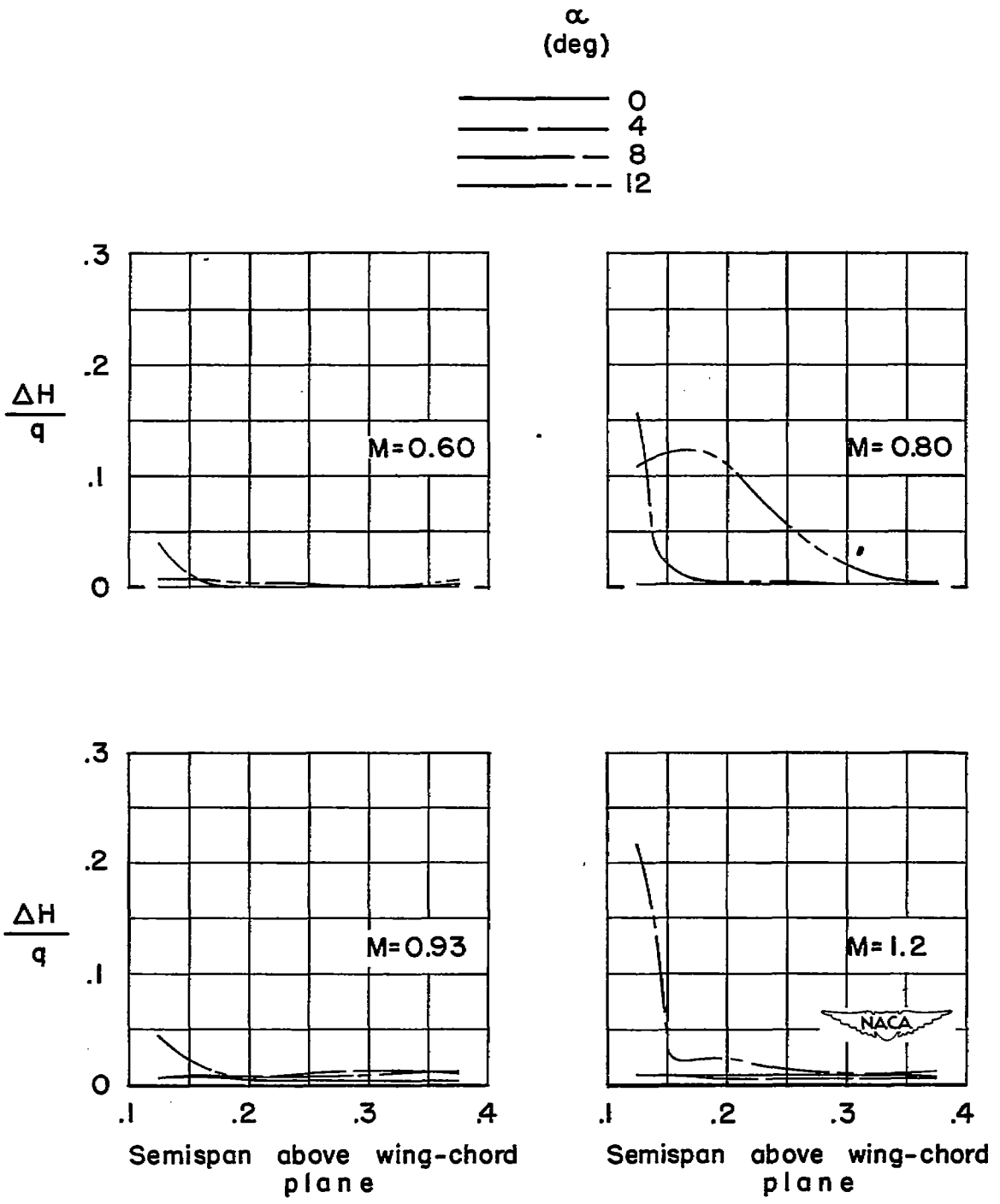

(b) 0.292 semispan from plane of symmetry.

Figure 16.- Concluded.

[redacted]

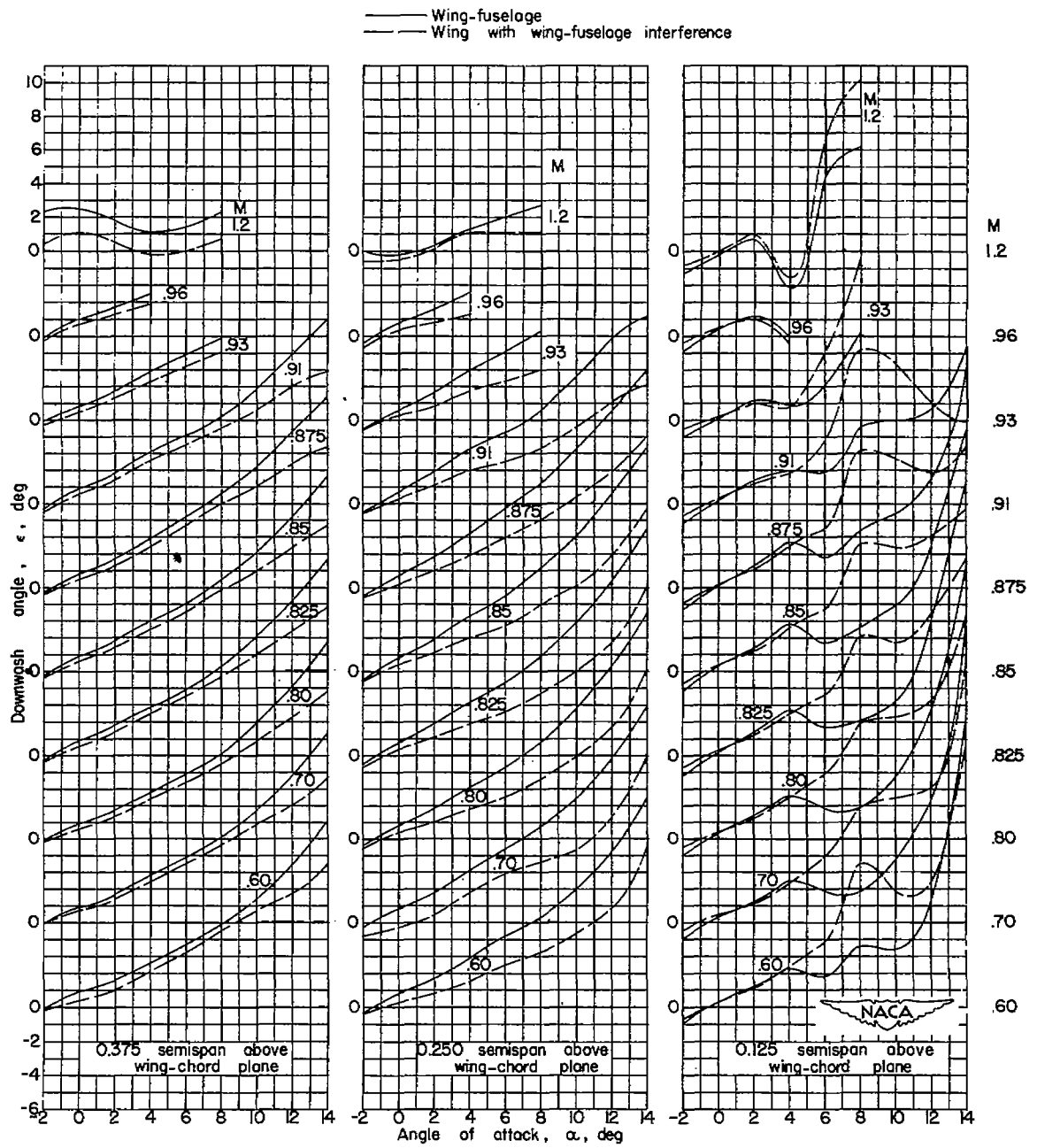

(a) Location 0.083 semispan from plane of symmetry.

Figure 17.- Variation of downwash angle with angle of attack at a point 1.225 semispans behind the wing 0.25$\bar{c}$ location for the wing-fuselage configuration and the wing with wing-fuselage interference.

[redacted]

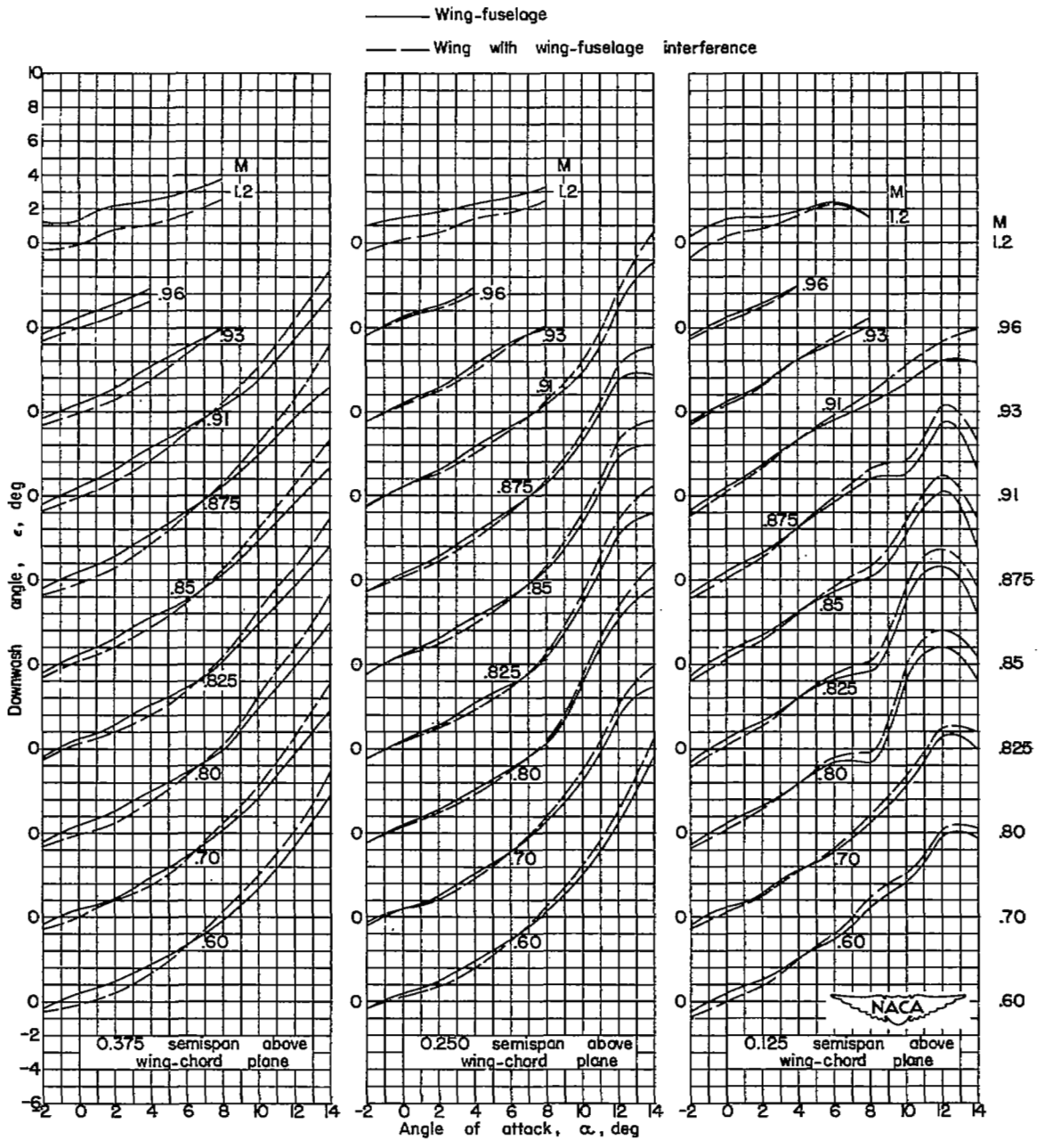

(b) Location 0.292 semispan from plane of symmetry.

Figure 17.- Concluded.

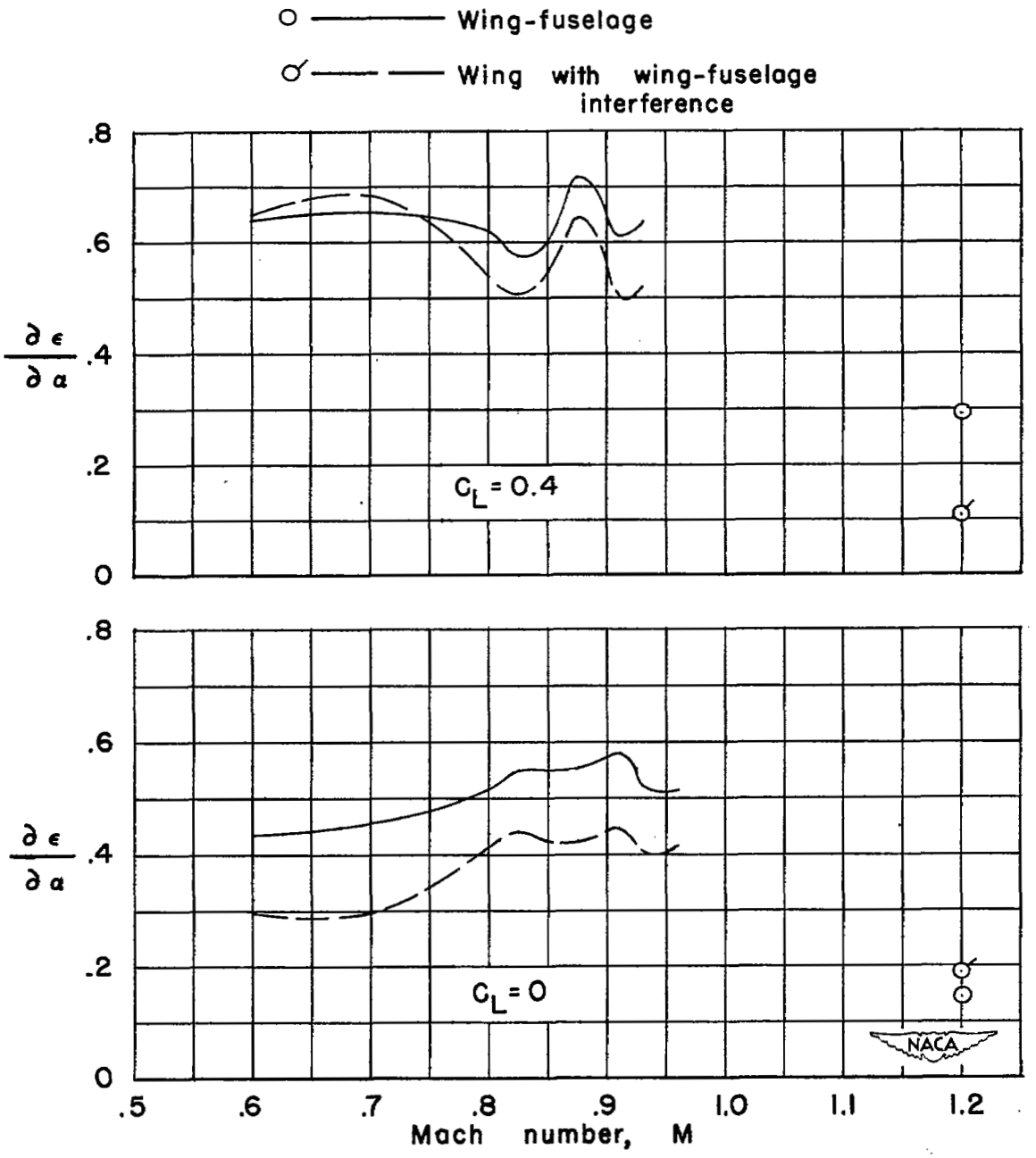

Figure 18.- Average spanwise downwash gradient at a height 0.25 semispan above the wing-chord plane as a function of Mach number for the wing-fuselage configuration and the wing with wing-fuselage interference.